Development and utility of a PAK1-selective degrader

Hoi-Yee Chow[1*], Sofiia Karchugina[1*], Brian J. Groendyke[2,4*], Sean Toenjes[5], John Hatcher[2], Katherine A. Donovan[2,3], Eric S. Fischer[2,3], Gleb Abalakov[1], Bulat Faezov[1], Roland Dunbrack[1], Nathanael S. Gray[5#], and Jonathan Chernoff[1,6#]

1 Fox Chase Cancer Center, Philadelphia, PA
2 Department of Cancer Biology; Dana Farber Cancer Institute, Boston, MA
3 Department of Biological Chemistry and Molecular Pharmacology, Harvard Medical School, Boston, MA
4 Current address: Blueprint Medicines, Cambridge, MA
5 Department of Chemical and Systems Biology, Chem-H and Stanford Cancer Institute, Stanford School of Medicine, Stanford University, Stanford, CA
6 Corresponding author: Jonathan Chernoff, Cancer Signaling and Epigenetics Program, Fox Chase Cancer Center, Philadelphia, Pennsylvania 19111, United States http://orcid.org/0000-0002-4803-7836; Email: Jonathan.Chernoff@fccc.edu

*These authors contributed equally to this work
Co-senior authors

Abstract

Amplification and/or overexpression of the *PAK1* gene is common in several malignancies, and inhibition of PAK1 by small molecules has been shown to impede the growth and survival of such cells. Potent inhibitors of PAK1 and its close relatives, PAK2, and PAK3, have been described, but clinical development has been hindered by recent findings that PAK2 function is required for normal cardiovascular function in adult mice. A unique allosteric PAK1-selective inhibitor, NVS-PAK1-1, provides a potential path forward, but has relatively modest potency in cells. Here, we report the development of BJG-05-039, a PAK1-seletive degrader consisting of the allosteric PAK1 inhibitor NVS-PAK1-1 conjugated to lenalidomide, a recruiter of the E3 ubiquitin ligase substrate adaptor Cereblon (CRBN). BJG-05-039 induced degradation of PAK1, but not PAK2, and displayed enhanced anti-proliferative effects relative to its parent compound in PAK1-dependent, but not PAK2-dependent, cell lines. Notably, BJG-05-039 promoted sustained PAK1 degradation and inhibition of downstream signaling effects at ten-fold lower dosage than NVS-PAK1-1. Our findings suggest that selective PAK1 degradation may confer more potent pharmacological effects compared with catalytic inhibition and highlight the potential advantages of PAK1-targeted degradation.

INTRODUCTION

p21-activated kinases (PAKs) have been considered as potential drug targets in a variety of cancers [1-4]. The PAK family is comprised of two groups: group A (PAK1, -2, and -3) and Group B (PAK4, -5-, and -6)[5]. The three members of the Group A PAKs are all closely related in sequence and structure, whereas the three Group B PAKs are distinct from the Group A proteins as well as more distantly related to one another. In addition to their structural differences, the six isoforms have distinct though sometimes overlapping expression patterns. For example, PAK1 is primarily expressed in brain, muscle, and blood cells, PAK2 is ubiquitous, and PAK3 is primarily expressed in neuronal cells. Of the Group B PAKs, PAK4 is ubiquitous, PAK5 is expressed mainly in neuronal cells, and PAK6 is expressed in neuronal cells, skin, prostate and testes [4, 6]. Genetic loss-of-function analyses in animal models has shown a variety of different phenotypes, ranging from embryonic lethality (PAK2, PAK4), to cognitive dysfunction (PAK3), to minimal effects (PAK1, PAK5, PAK6) [7, 8].

As effectors of the small GTPase RAC, the PAK enzymes regulate several key proliferative and survival pathways including the RAF-MEK-ERK, the PI3K-AKT-mTORC, and the β-catenin pathways [2]. While rarely subject to mutational activation, certain PAK isoforms, in particular PAK1 and PAK4, are frequently expressed at high levels in various tumor types due to chromosomal amplifications of their corresponding genes at chromosome 11q13 and 19q13, respectively [2, 3], or are activated by mutations in RAC1 [9]. Reducing PAK activity, via gene knockouts, RNA interference, or small molecule inhibitors, has been shown to be of benefit in many cell-based and *in vivo* cancer models [2]. These factors led several pharmaceutical companies to develop various PAK inhibitors for cancer therapy [10-14]. One of these, Pfizer's pan-PAK inhibitor PF3758309, was evaluated in a human Phase 1 clinical trial, but was withdrawn due to a combination of poor pharmaceutical properties and toxicity [2]. Afraxis and Genentech described a series of increasingly specific Group A PAK inhibitors, which were found to be effective in preclinical models of NF2, KRAS-driven squamous cell carcinoma, and HER2-driven breast cancer [11, 15-17]. However, development of this series of compounds was halted in 2016 due to evidence of on-target toxicity related to cardiovascular events [14]. Similar findings were described in *Pak2* knockout mice, using a tamoxifen regulated CAGG-Cre-ERT gene to delete the floxed *Pak2* gene in adult mice [18]. In contrast, deletion of the closely related genes for *Pak1* and *Pak3* was not found to be required for viability, development, longevity, or fertility [7, 19]. These combined findings suggested that PAK2 function is required in adult mice and that small molecules that inhibit PAK2 might be toxic or even lethal in humans, muting enthusiasm for further development of Group A PAK inhibitors.

In 2015, Novartis described a dibenzodiazepine-based small molecule inhibitor, NVS-PAK1-1, that showed excellent specificity for PAKs over other kinases and a ~50x selectivity for PAK1 over PAK2 [20]. Given the extensive similarity between the catalytic domains of PAK1 and PAK2 (93% identical), this selectivity was unexpected, as was the co-crystal structure which revealed that the molecule occupied a space in the catalytic cleft underneath the αC-helix rather than in the hinge region of the ATP binding pocket. Selective blockade of PAK1 might be clinically useful in an animal model of NF2, as we recently reported that deletion of the *Pak1*, but not the

Pak2 gene, was effective in slowing hearing loss and schwannoma growth in these mice, and that treatment with NVS-PAK1-1 showed a similar trend without obvious systemic toxicity [21]. As several cancer cells are PAK1-dependent, these findings suggested a path forward for PAK1-selective inhibitors. However, NVS-PAK1-1 has a short half-life in rat liver microsomes and, *in vivo*, is metabolized by the cytochrome P450 system [20, 21]. To our knowledge, only one other class of small molecule inhibitors has displayed a similar selectivity for PAK1 over PAK2, which is achieved by binding to the less conserved p21-binding domain at the N-terminus of PAK1, as opposed to the highly conserved kinase domain [22]. However, these compounds are only effective at micromolar doses.

Given that the signaling activity of PAK1 is mediated both by enzymatic and scaffolding functions [6, 23], we considered that a degrader derived from NVS-PAK1-1 might prove more potent than the parental molecule, while simultaneously retaining its selectivity for PAK1 over PAK2. We therefore synthesized and characterized a small collection of bivalent degraders (PROTACs) derived from conjugating NVS-PAK1-1 to lenalidomide which facilitate recruitment of the $CRL4^{CRBN}$ ubiquitin ligase for substrate ubiquitination and eventual proteosome-mediated degradation. We anticipated that this bivalent degrader would preserve the unique isoform-specific PAK1 inhibitor activity while simultaneously being capable of inducing PAK1 protein degradation. In this report, we describe the properties of an optimized PAK1-specific degrader, as compared to the parental inhibitor, a negative degrader (analog disabled for binding to CRBN), and to shRNA-mediated gene knockdown. We found that the degrader form of NVS-PAK1-1 could be used at ten-fold lower doses to reduce growth signaling and proliferation of PAK1-dependent, but not PAK2-dependent cell lines. These effects could be enhanced by co-treatment with a drug efflux inhibitor. These results represent the first degrader form of a PAK inhibitor, and could form the basis for future development of PAK1-specific inhibitors.

RESULTS AND DISCUSSION

Design of a Selective PAK1 Degrader. To develop a PAK1-selective heterobifunctional degrader, we designed compounds based on NVS-PAK1-1, a unique allosteric inhibitor which displays marked selectivity for PAK1 over PAK2 (Figure 1A) [20]. This compound is based on a dibenzodiazepine scaffold, which is uncommon for kinase inhibitors. Co-crystals of close relatives of NVS-PAK1-1 show that these molecules bind beneath the αC helix in PAK1 in a pocket formed in the DFG-out conformation of PAK1 analogous to the well-characterized allosteric inhibitors of MEK1/2 [24] and EGFR [25]. It has been speculated that they derive specificity for PAK1 over PAK2 due to a steric clash between the molecule with Leu301 in PAK2 *vs.* the equivalent Asn322 in PAK1 [20] (Figure 1B). Such specificity is unusual and has rarely been described for other inhibitors of Group A PAK. For example, we tested NVS-PAK1-1 and over 2000 hinge-region kinase inhibitors against PAK1 and PAK2 using an in vitro kinase assay. With the exception of NVS-PAK1-1, none of the other compounds displayed differential sensitivities between these two kinases (Figure 1C).

As NVS-PAK1-1 has a short *in vivo* half-life and has shown marginal effects in cancer cell lines [20], we attempted to create degrader forms of this compound. Such compounds might have the added advantage over conventional PAK inhibitors because, in addition to blocking kinase

enzymatic activity, they also have the potential to reduce signaling effects that emanate from the scaffold functions of PAK1. A co-crystal structure of a close analogue of NVS-PAK1-1 bound to PAK1 (PDB: 4ZJJ) revealed that the isopropyl urea is solvent exposed, suggesting that the carbonyl (either as a urea or an amide) could serve as a suitable attachment site for linkers without adversely affecting affinity to PAK1 (Figure 1E).

Hydrocarbon and polyethylene glycol (PEG) linkers of varying lengths were used to conjugate NVS-PAK1-1 with either a CRBN ligand (lenalidomide) or a VHL ligand, respectively. To verify that conjugation of the linker and lenalidomide or VHL ligand did not affect the ability of NVS-PAK1-1 to bind to PAK1, ten different NVS-PAK1-1 conjugates were tested in a commercially available fluorescence resonance energy transfer-based assay (Invitrogen, Z′-Lyte) for PAK1, PAK2, and PAK4 inhibition (Table S1). Three of these – BJG-05-014, BJG-05-027, and BJG-05-039 – retained PAK1 inhibitory activity and selectivity and were therefore selected for more detailed studies. While BJG-05-039 had lower inhibitory activity against PAK1 (half maximal inhibitory concentration (IC_{50}) = 233 nM) compared to NVS-PAK1-1 (IC_{50} = 29.6 nM), it displayed greater specificity (PAK2 IC_{50} > 10,000 nM for BJG-05-039 *vs.* 824 nM for NVS-PAK1-1), demonstrating that BJG-05-039 had improved selectivity for PAK1 over PAK2 compared to the parent molecule. Molecular modeling suggests that the addition of the linker and degrader moieties would not impair selective binding of the inhibitory ligand in the ATP cleft of PAK1 (Figure S1).

BJG-05-014, BJG-05-027, and BJG-05-03 were tested in Panc1 cells for their ability to degrade PAK1. Of these three molecules, BJG-05-039, which uses an 8-carbon linker to conjugate NVS-PAK1-1 with lenalidomide, had the most promising profile (Figure S2).

We evaluated the biochemical selectivity of BJG-05-039 against a panel of 468 kinases at 10 μM (KINOMEscan) and observed that BJG-05-039 had a similar selectivity profile as 10 μM NVS-PAK1-1 (Figure S3 and Table S2).

BJG-05-039 is a Highly Selective PAK1 Degrader. After verifying that BJG-05-039 retained specificity for PAK1, we sought to characterize its degradation activity in cells. We first chose to evaluate the PAK1 degrader in breast cancer cell line MCF7 and the ovarian cancer cell line OVCAR3 due to their high expression of both PAK1 and PAK2, and their known dependence on PAK1 [26, 27]. We found that BJG-05-039 induced degradation of PAK1 but not PAK2 in a dose-dependent manner after a 12 h treatment, with maximal degradation observed at 10 nM (Figure 2A). At concentrations of 1 μM and greater, we observed diminished PAK1 degradation, consistent with the hook effect, in which independent engagement of PAK1 and CRBN by BJG-05-039 prevents formation of a productive ternary complex [28]. PAK1 degradation was not observed in cells treated with the parent molecule, NVS-PAK1-1, or with BJG-05-098, a negative control compound with an N-methylated glutarimide that weakens CRBN binding (Figure 2A), demonstrating that BJG-05-039-induced PAK1 degradation was CRBN dependent [29]. Time course treatment of MCF7 cells with 250 nM BJG-05-039 revealed partial degradation of PAK1 within 4 h and progressive loss out to 24 h (Figure 2B). Co-treatment of cells with BJG-05-039 and bortezomib, a proteasome inhibitor, or MLN4924, an NAE1 (NEDD8-activating enzyme 1) inhibitor that prevents the neddylation required for the activation of cullin

RING ligases, such as $CRL4^{CRBN}$ [30], prevented PAK1 destabilization, indicating that degradation was dependent on the ubiquitin-proteasome system (Figure 2C).

To assess degrader selectivity across the proteome, MOLT4 cells were treated with 1 μM BJG-05-039 for 5 h and global multiplexed mass spectrometry-based proteomic analysis was performed [31]. As expected for lenalidomide-based degraders, the ring-finger protein RNF166 as well as other known IMiD off target proteins, Ikaros (IKZF1) and Aiolos (IKZF3), were strongly downregulated by BJG-05-039 treatment (Figure S4) [32]. Interestingly, while BJG-05-039 showed potent *in vitro* inhibition of PAK1 (IC_{50} = ss nM) and a ~50% reduction in PAK1 levels as determined by immunoblot (Figure 2A), significant downregulation of this kinase was not apparent in the proteomic analysis (Table S3).

To better quantify the effect of degrader treatment, we transfected HEK293 cells with an expression vector encoding nano-luciferase (Nluc)-tagged PAK1. The Nluc tag allows for luciferase-based quantitation of protein expression [33]. Nluc-PAK1 cells were treated with BJG-05-039 or its N-methylated analog, BJG-05-098 and PAK1 expression was assessed (Figure 2D). This experiment showed that half-maximal degradation of PAK1 was achieved at low nM concentrations of BJG-05-039, with approximately 70% reduction in PAK1 expression following treatment with 10 nM of BJG-05-039.

BJG-05-039 Exhibits Enhanced Effects on Signaling Compared with NVS-PAK1-1. In certain cell lines PAK1 has well-characterized functions in regulating proliferative signaling. We compared the activity of BJG-05-039 against NVS-PAK1-1 in two such cell lines, OVCAR3 and MCF7. As a readout for anti-PAK activity, we assessed phosphorylation of MEK1 at S298, a direct target site for Group A PAKs [34], as well as phosphorylation of the downstream target of MEK, ERK. At a 10 nM dose, BJG-05-039 inhibited phosphorylation of MEK S298, as well as inhibiting phosphorylation of ERK, however an equivalent dose of NVS-PAK1-1 had no visible impact on phosphorylation status of these proteins (Figure 3A). Selective knockdown of PAK1 showed similar effects to BJG-05-039 in these cell lines, substantially reducing levels of phospho-MEK and phospho-ERK, whereas knockdown of PAK2 showed little effect (Figure 3B).

BJG-05-039 is Effective in Reducing Proliferation in PAK1-Dependent, but not PAK2-Dependent Cell Lines. We next compared the anti-proliferative effects of PAK1 degradation and inhibition. Using the same two cell lines, we found that BJG-05-039 was far more potent than NVS-PAK1-1, with EC_{50} values of 3 and 8.4 nM in MCF7 and OVCAR3 cells, respectively, compared to 11.9 μM and 3.68 μM, respectively, for the parental compound NVS-PAK1-1 (Figure 4A and 4B). In contrast, BJG-05-039 did not show increased efficacy relative to NVS-PAK1-1 in OMM1 and HEY-A8 cells, which genome-wide CRISPR-screens suggest are highly dependent on PAK2 (Figure 4A and 4B) (https://depmap.org/portal/gene/PAK2?tab=dependency). These large differences in EC_{50} values in PAK1-dependent cells are likely to be ddirectly related to the degrader properties of BJG-05-039, as an isomeric non-degrader control (BJG-05-098) shoed no activity in any of the cell lines (Fig. 4C). In addition, the effects of BJG-05-039 are unlikely to be caused by non-specific degradation of proteins (*e.g.*, IKZF1 or IKZF3), as lenalidomide lacked significant antiproliferative effects in either cell line (Figure 4D). These data suggest that the combined

selective inhibition and degradation of PAK1 by BJG-05-039 is more potent at reducing proliferative signaling in PAK1-dependent cells than what can be achieved by inhibiting catalytic activity alone. Consistent with this view, NVS-PAK1-1 showed much more potent anti-proliferative effects in cells in which PAK1 levels were reduced ~50% using shRNA (Figure 4E). These results also support a mechanism of action related to combined PAK1 inhibition/degradation as opposed to "off-target" degradation effects.

In many cancer cells, Group A PAKs act as signaling hub, coordinating the activation of various central proliferative, survival, and motility pathways [2]. As such, there has been interest in targeting these enzymes with small molecule inhibitors [10, 12, 35]. One pan-PAK inhibitor, PF3758309 [10], was evaluated in a phase 1 clinical trial, but poor pharmacologic properties and excessive toxicity led to its withdrawal. More selective inhibitors, such as FRAX-597, FRAX-1036, and G5555 showed efficacy in cell-based models, in particular, in cells in which the *PAK1* gene was amplified or in which *RAC1* was a driving oncogene [11-13, 16, 27, 36]. However, progress in clinical development has been hampered by genetic and pharmacologic evidence suggesting a vital role for PAK2 in cardiovascular function and vascular integrity in adult mammals [14, 18]. Acute cardiotoxicity upon inhibitor treatment or gene loss is thought to be due to a unique role for PAK2 in regulating ER stress and oxidative stress in cardiomyocytes [37].

While the vast majority of Group A PAK inhibitors equally affect PAK1, -2, and -3, NVS-PAK1-1 - an allosteric inhibitor that binds beneath the αC helix rather than in the hinge region of the ATP binding pocket of PAK1 - exhibits an approximately 50-fold specificity for PAK1 over PAK2. This unique specificity prompted us to ask if we could improve upon this molecule by imparting it with the ability to degrade its target. As with FAK degraders [38], PAK1 degraders have the potential to incite more benefit than standard enzymatic inhibitors because removal of PAK1 would not only reduce its kinase enzymatic activity, but also its scaffolding function, both of which mediate signaling activity. For example, PAK1 has been shown to be required for AKT activation [15, 39], but these effects map to the N-terminus of PAK1 and appear to be independent of kinase activity [39]. Degraders also offer the potential for prolonged efficacy, which is driven by target half-life, and this is an important consideration given the short half-life of NVS-PAK1-1 [20, 21]. While adding the linker and lenalidomide moiety to NVS-PAK-1 reduced the potency of BJG-05-039 as a PAK1 catalytic inhibitor, it also increased its selectivity over PAK2 more than ten-fold (Table S1). Given the necessity for isoform selective targeting, this improved selectivity for PAK1 could reduce the potential toxicity of this molecule relative to the parental NVS-PAK1-1.

While we were not able to achieve more than 70% loss of the PAK1 protein using BJG-05-039, the combination of catalytic inhibition and lowered protein expression had dramatically improved inhibitory effects on signaling and proliferation in PAK1-dependent cell lines (Figures 3A and 4A). In this respect, the degrader may be mimicking the effects of genetic manipulations such as RNAi-mediated gene knock down. This property can be used, in conjunction with the parental inhibitor NVS-PAK1-1, to tease apart kinase *vs.* scaffolding effects of PAK1 in cells. In fact, our data suggests that reducing the total level of PAK1 expression synergizes with catalytic expression, as evidenced by the increased potency of the non-degrader NVS-PAK-1 when used in conjunction with partial knockdown of PAK1 with shRNA (Figure 4C). Thus, in addition to

its potential role in reigniting interest in clinical development of PAK inhibitors, the degrader compound described herein provides a useful tool compound for signaling analysis.

CONCLUSION

Given their role in regulating the ERK, AKT, and b-catenin pathways, Group A PAKs have been considered as potential therapeutic targets in cancer. However, the PAK2 isoform plays a key role in normal cardiovascular function in adult mammals, and this factor has impeded further preclinical development of anti-PAK agents. Selective PAK2-sparing molecules present a potential path forward and we previously showed that one such inhibitor, NVS-PAK1-1, has promising effects in a mouse model of NF2. Given that PAK1 has significant scaffolding activity in addition to its catalytic activity, we considered that a degrader based on NVS-PAK1-1 might provide considerable benefits while avoiding toxicities associated with PAK2 inhibition. Here, we show that an optimized heterobifunctional degrader, BJG-05-039, promoted rapid and selective degradation of PAK1 but not PAK2, and had more potent anti-proliferative effects than NVS-PAK-1. Given that many cancer cell types display elevated PAK1 expression and activity, and knockdown of PAK1 has been shown to have considerable anti-proliferative and/or anti-survival effects in these settings, isoform-specific inhibition and degradation of PAK1 may reignite interest in targeting this kinase in cancer.

EXPERIMENTAL SECTION

Chemical Synthesis. Detailed information on chemical synthesis analytical data as well as supplementary data can be found in the Supporting Information.

Cell Lines, MCF7 (female, CVCL_0031) and HEK293 cells were cultured in high-glucose DMEM medium (Gibco) supplemented with 10% fetal bovine serum (HyClone), 2 mM L-glutamine and 100U/ml penicillin/streptomycin (Gibco). MOLT4 (male, CVCL_0013) were cultured in RPMI 1640 medium (Gibco) supplemented with 10% fetal bovine serum and 2 mM L-glutamine. OVCAR3 (female, CVCL_0465), Hey A8 (female, CVCL_8878) and OMM1 (male, CVCL_6939) were cultured in RPMI 1640 medium (Gibco) supplemented with 10% fetal bovine serum, 2 mM L-glutamine and 100U/ml penicillin/streptomycin (Gibco). All cell lines were cultured at 37°C in a humidified 5% CO_2 incubator. HEK293 cells stably expressing Nluc-PAK1 were constructed by transfecting with the pFN31K Nluc-PAK1 expression vector (0.5 μg DNA per well) in 12-well plates using Lipofectamine 3000 (Invitrogen) according to the manufacturer's protocol. Transfected Nluc-PAK1 cells were cultured for 1 week in DMEM medium containing G418 (2 mg ml^{-1}) to select stable clones.

A doxycycline (Dox)-inducible shRNA-bearing retrovirus against PAK1 was previously described[27] and oligonucleotide used in this study are as follows: PAK1 shRNA-1 5′-GAT CCCCGAAGAGAGGTTCAGCTAAATTCAAGAGATTTAGCTGAACCTCTCTTCTTTTTT GGAAA-3′; Recombinant viruses were generated using the Phoenix amphotropic packaging system (Orbigen). the ΦNX cells were transfected using Lipofectamine 3000 (Invitrogen). Viral supernatants were harvested 72 hr post-transfection and filtered. Ovarian (OVCAR3) and breast (MCF7) cancer cells were incubated with retroviral supernatant supplemented with 8 μg/ml polybrene for 4 h at 37°C, and then were cultured in growth media for 48 h for viral integration. Green fluorescent protein (GFP)-positive infected cells were selected by flow cytometry.

Plasmids, The pFN31K-Nluc-PAK1 vector was constructed as follows: The gene sequence encoding PAK1 from pCMV6M-PAK1 (Plasmid #12209 Addgene) was PCR-amplified using the following oligonucleotide pair:
TTCTGGCGGGCTCGAGCGTCGACATGGAACAGAAACT (Forward),
TACCGAGCCCGAATTGAATTCCTCGAGGCCACGAAG (Reverse), designed with recognition sites for XhoI and EcoRI restriction enzymes. The PCR product was subcloned into the expression vector pFN31K-Nluc) using the XhoI and EcoRI restriction endonucleases (NEB, USA) and In-Fusion HD Enzyme (Takara, Japan).

Retroviral transductions. The ΦNX packaging cell line (Orbigen) was transfected using Lipofectamine 2000 (ThermoFisher Scientific) according to the manufacturer's instruction. Viral supernatants were harvested 48 hours post-transfection and filtered. Cells were incubated with retroviral supernatant supplemented with 4 μg/ml polybrene for 4 hours at 37°C, and then were cultured in growth media for 48 hours for viral integration. Green fluorescent protein (GFP)-positive infected cells were selected by flow cytometry.

Drug Treatment with PAK1 Degraders. NVS-PAK1-1, BJG-05-039, BJG-05-098, bortezomib (Selleckchem), and lenalidomide (Selleckchem) were dissolved in DMSO at 10 mM. Cells were seeded in 6-well plate at 250,000 cells per mL in 2 mL per well. Cells were incubated overnight then treated with various concentrations of PAK degraders alone or together with bortezomib or lenalidomide for 24 hours. Protein lysates were harvested at the times specified.

Immunoblotting. Cells were washed once in PBS and lysed in RIPA buffer (50 mM Tris-HCl, 150 mM NaCl, 0.25% (w/v) sodium deoxycholate, 1% (w/v) NP-40, pH 7.5) containing protease inhibitor cocktail (Roche) and phosphatase inhibitor cocktail (Roche) for 30 minutes on ice. Cell lysates were obtained by centrifugation at 13,500 rpm for 15 minutes at 4°C. BCA protein assay (Thermo Scientific) was used to determine protein concentration then equal amounts of total proteins were separated by SDS-PAGE (Bio-Rad) and transferred to PVDF membrane (Thermo Scientific) at 100V for 2 hours. Membranes were blocked in 5% (w/v) non-fat dry milk in tris-buffered saline with 0.1% Tween-20 (TBS-T) for 1 hour and incubated with primary antibody at 4°C for overnight. Membranes were washed with TBS-T on the next day and incubated with HRP-conjugated secondary antibodies (Millipore) at room temperature for 1 hour and exposed to films after washing.

Antibodies	Company	Catalog	Dilution
Rabbit PAK1	Cell Signaling Technology	2602	1:1000
Rabbit PAK2	Cell Signaling Technology	2608	1:1000
Rabbit MEK	Cell Signaling Technology	9122	1:1000
Rabbit Phospho-MEK	Cell Signaling Technology	9128	1:1000
Rabbit ERK	Cell Signaling Technology	4695	1:2500
Rabbit Phospho-ERK	Cell Signaling Technology	9101	1:2500
Rabbit GAPDH	Cell Signaling Technology	2118	1:2500
Mouse Vinculin	Sigma-Aldrich	V9131	1:2000

Cell viability assay. Cells were plated at 2 x 10^3 cells per well in 96-well plates overnight and treated with various concentrations of Pak degraders for 72 hours. Cell viability was

measured by MTT assay and the half maximal inhibitory concentration (IC_{50}) was calculated using GraphPad Prism. Triplicates were performed for each sample and medium alone was used as a blank.

Luciferase Assays. HEK293 cells stably expressing pFN31K-Nluc-PAK1 were assayed for luciferase activity according to the manufacturer's Nano-Glo® Live Cell Assay System protocol (Promega). In brief, 25µl of Nano-Glo Live Cell Reagent was added per well and the plate was gently mixed by hand, then placed in a 37°C luminometer for 10 minutes.

KinomeScan. The kinase engagement assay (KINOMEscan) was performed by DiscoverX assessing binding abilities toward a set of protein kinases. NVS-PAK1-1 was screened at a concentration of 1 µM and BJG-05-039 was screened at a concentration of 10 µM.

Kinase Activity Assay. Kinase activity assays were performed by Reaction Biology Corp. Compounds were tested in 10-dose IC50 duplicate mode with a 3-fold serial dilution starting at 1 µM. The control compound, staurosporine, was tested in 10-dose IC50 mode with 4-fold serial dilution starting at 20 µM. Reactions were carried out at 10 µM ATP. IC50 values were calculated using Prism 7.0 (GraphPad)

Biochemical Assay Protocol for PAK1 and PAK2. The activity/inhibition of human recombinant PAK1 (kinase domain) or PAK2 (full length) was determined by measuring the phosphorylation of a FRET peptide substrate (Ser/Thr19) labeled with Coumarin and Fluorescein using Z'-LYTE™ assay (Invitrogen). The 10 µL assay mixtures contained 50 mM HEPES (pH 7.5), 0.01% Brij-35, 10 mM $MgCl_2$, 1 mM EGTA, 2 µM FRET peptide substrate, and PAK enzyme (20 pM PAK1; 50 pM PAK2). Incubations were carried out at 22°C in black polypropylene 384-well plates (Corning Costar). Prior to the assay, enzyme, FRET peptide substrate and serially diluted test compounds were preincubated together in assay buffer (7.5 µL) for 10 minutes, and the assay was initiated by the addition of 2.5 µL assay buffer containing 4x ATP (160 µM PAK1; 480 µM PAK2). Following the 60-minute incubation, the assay mixtures were quenched by the addition of 5 µL of Z'-LYTE™ development reagent, and 1 hour later the emissions of Coumarin (445 nm) and Fluorescein (520 nm) were determined after excitation at 400 nm using an Envision plate reader (Perkin Elmer). An emission ratio (445 nm/520 nm) was determined to quantify the degree of substrate phosphorylation.

TMT LC-MS Sample Preparation. MOLT4 cells were treated with DMSO in biological triplicate and 1 µM BJG-05-039 for 5 h and harvested by centrifugation. Cell lysis was performed by the addition of Urea buffer (8 M Urea, 50 mM NaCl, 50 mM 4-(2-hydroxyethyl)-1-piperazineethanesulfonic acid (EPPS) pH 8.5, Protease and Phosphatase inhibitors) followed by manual homogenization by 20 passes through a 21-gauge (1.25 in. long) needle. Lysate was clarified by centrifugation at 4 °C and protein quantified using bradford (Bio-Rad) assay. 100 μg of protein for each sample was reduced, alkylated and precipitated using methanol/chloroform as previously described [31]. The resulting precipitated protein was resuspended in 4 M Urea, 50 mM HEPES pH 7.4, buffer for solubilization, followed by dilution to 1 M urea with the addition of 200 mM EPPS, pH 8. Proteins were digested for 12 hours at room temperature with LysC (1:50 ratio), followed by dilution to 0.5 M urea and a second digestion step was performed by addition of trypsin (1:50 ratio) for 6 hours at 37 ºC. Anhydrous ACN was added to each peptide sample to

a final concentration of 30%, followed by addition of Tandem mass tag (TMT) reagents at a labelling ratio of 1:4 peptide:TMT label. TMT labelling occurred over a 1.5 h incubation at room temperature followed by quenching with the addition of hydroxylamine to a final concentration of 0.3%. Each of the samples were combined using adjusted volumes and dried down in a speed vacuum followed by desalting with C18 SPE (Sep-Pak, Waters). The sample was offline fractionated into 96 fractions by high pH reverse-phase HPLC (Agilent LC1260) through an aeris peptide xb-c18 column (phenomenex) with mobile phase A containing 5% acetonitrile and 10 mM NH_4HCO_3 in LC-MS grade H_2O, and mobile phase B containing 90% acetonitrile and 5 mM NH4HCO3 in LC-MS grade H_2O (both pH 8.0). The resulting 96 fractions were recombined in a non-contiguous manner into 24 fractions and desalted using C18 solid phase extraction plates (SOLA, Thermo Fisher Scientific) followed by subsequent mass spectrometry analysis.

Data were collected using an Orbitrap Fusion Lumos mass spectrometer (Thermo Fisher Scientific, San Jose, CA, USA) coupled with an Proxeon EASY-nLC 1200 LC lump (Thermo FIsher Scientific, San Jose, CA, USA). Peptides were separated on a 50 cm 75 μm inner diameter EasySpray ES903 microcapillary column (Thermo Fisher Scientific). Peptides were separated over a 190 min gradient of 6 - 27% acetonitrile in 1.0% formic acid with a flow rate of 300 nL/min.

Quantification was performed using a MS3-based TMT method as described previously. The data were acquired using a mass range of m/z 340 – 1350, resolution 120,000, AGC target 5 x 105, maximum injection time 100 ms, dynamic exclusion of 120 seconds for the peptide measurements in the Orbitrap. Data dependent MS2 spectra were acquired in the ion trap with a normalized collision energy (NCE) set at 35%, AGC target set to 1.8 x 104 and a maximum injection time of 120 ms. MS3 scans were acquired in the Orbitrap with HCD collision energy set to 55%, AGC target set to 2 x 105, maximum injection time of 150 ms, resolution at 50,000 and with a maximum synchronous precursor selection (SPS) precursors set to 10.

LC-MS data analysis. Proteome Discoverer 2.4 (Thermo Fisher Scientific) was used for .RAW file processing and controlling peptide and protein level false discovery rates, assembling proteins from peptides, and protein quantification from peptides. The MS/MS spectra were searched against a Swissprot human database (December 2019) containing both the forward and reverse sequences. Searches were performed using a 20 ppm precursor mass tolerance, 0.6 Da fragment ion mass tolerance, tryptic peptides containing a maximum of two missed cleavages, static alkylation of cysteine (57.02146 Da), static TMT labelling of lysine residues and N-termini of peptides (304.2071 Da), and variable oxidation of methionine (15.99491 Da). TMT reporter ion intensities were measured using a 0.003 Da window around the theoretical m/z for each reporter ion in the MS3 scan. The peptide spectral matches with poor quality MS3 spectra were excluded from quantitation (summed signal-to-noise across channels < 100 and precursor isolation specificity < 0.5), and the resulting data was filtered to only include proteins with a minimum of 2 unique peptides quantified. Reporter ion intensities were normalized and scaled using in-house scripts in the R framework [41]. Statistical analysis was carried out using the limma package within the R [42].

Cell Viability and Luciferase Assays: All experiments were performed at least three times. Results were reported as means ± SD. The significance of the data was determined by two-tailed, unpaired Student's *t*-test with $p < 0.05$ considered statistically significant.

Data and code availability. The accession number for the proteomic data reported in this paper in Pride: PXcccc

Figure Legends

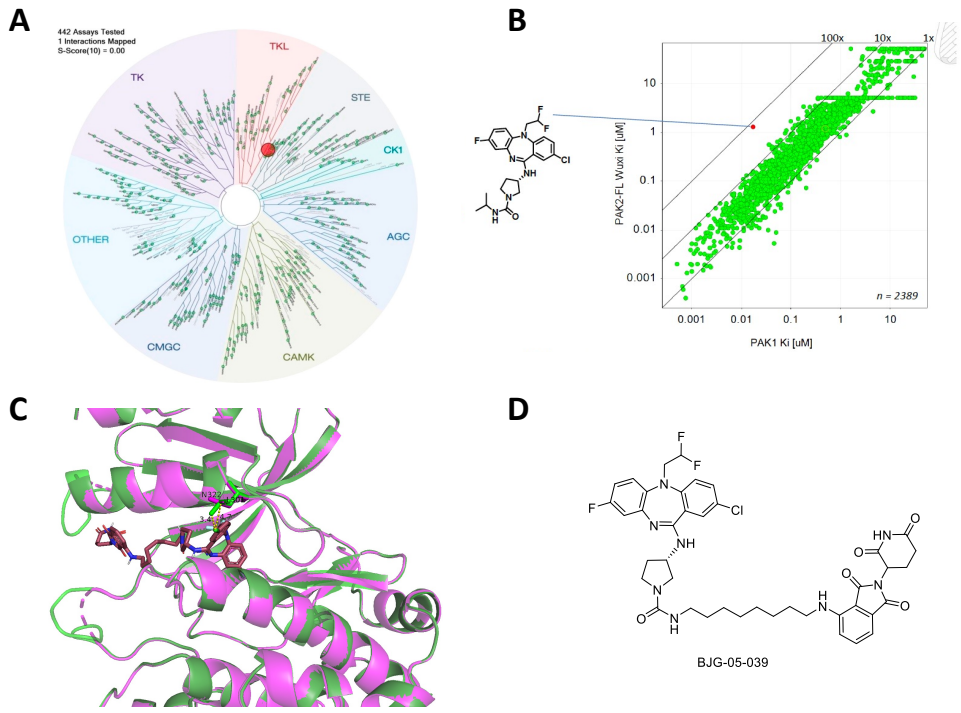

Chow et al Figure 1

Figure 1. Structure and Selectivity of PAK1 Degrader. A) TREEspot visualization of the biochemical kinome selectivity of 1 μM NVS-PAK1-1. **B)** Proposed structural basis for isoform specificity. The crystal structure of PAK1 is depicted in magenta (PDB entry, 4ZJI, chain A). PAK2 in green was modeled using Swiss-Model using 4ZJI chain A as a template. BJG-05-039 was modeled using Open Babel from its SMILES string and docked with AutoDock Vina. Amino acids that contact the ligand and differ between PAK1 and PAK2 are shown in sticks. N322 in PAK1 and L301 in PAK2 are labeled; the side chain of L301 forms a very close contact with the ligand (3.4 Å) compared to N322 in PAK1 (4.7 Å). **C)** Specificity of NVS-PAK1-1 compared to other Group A PAK inhibitors. *In vitro* kinase assays were performed using recombinant PAK1 and PAK2, using a library of 2389 hinge-binding small molecule protein kinase inhibitor compounds from Genentech's PAK1 inhibitor program, plus NVS-PAK1-1. **D)** Chemical structure of BJG-05-039.

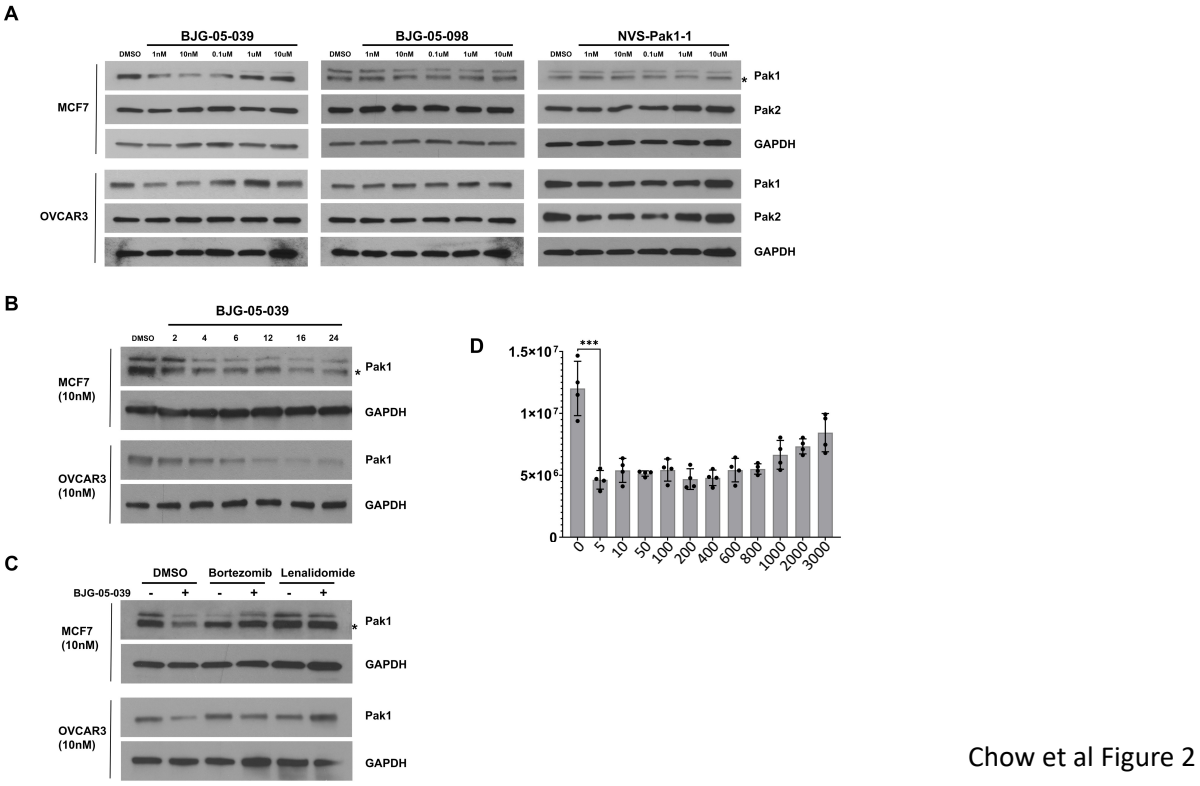

Chow et al Figure 2

Figure 2. BJG-05-039 Induces Selective Degradation of PAK1 Dependent on CRBN, Neddylation, and the Proteosome. A) Effects of BJG-05-039, BJG-05-098, and NVS-PAK1-1 on PAK1 and PAK2 expression. MCF7 and OVCAR3 cells were treated with increasing concentrations of the indicated compounds for 24 h and protein lysates were analyzed by immunoblot. **B)** Time course of PAK1 degradation. **C)** Effect of Bortezomib and Lenalidomide, respectively, on degrader capacity of BJG-05-039. Asterisk indicates PAK1 signal on immunoblot. **D)** Quantitation of PAK1 expression by luminescence assay. HEK293 cells stably expressing near-endogenous levels of Nluc-PAK1 were treated with the indicated concentrations of BJG-05-039. 24 h post treatment the cells were lysed an analyzed for luciferase activity as described in the Methods section.

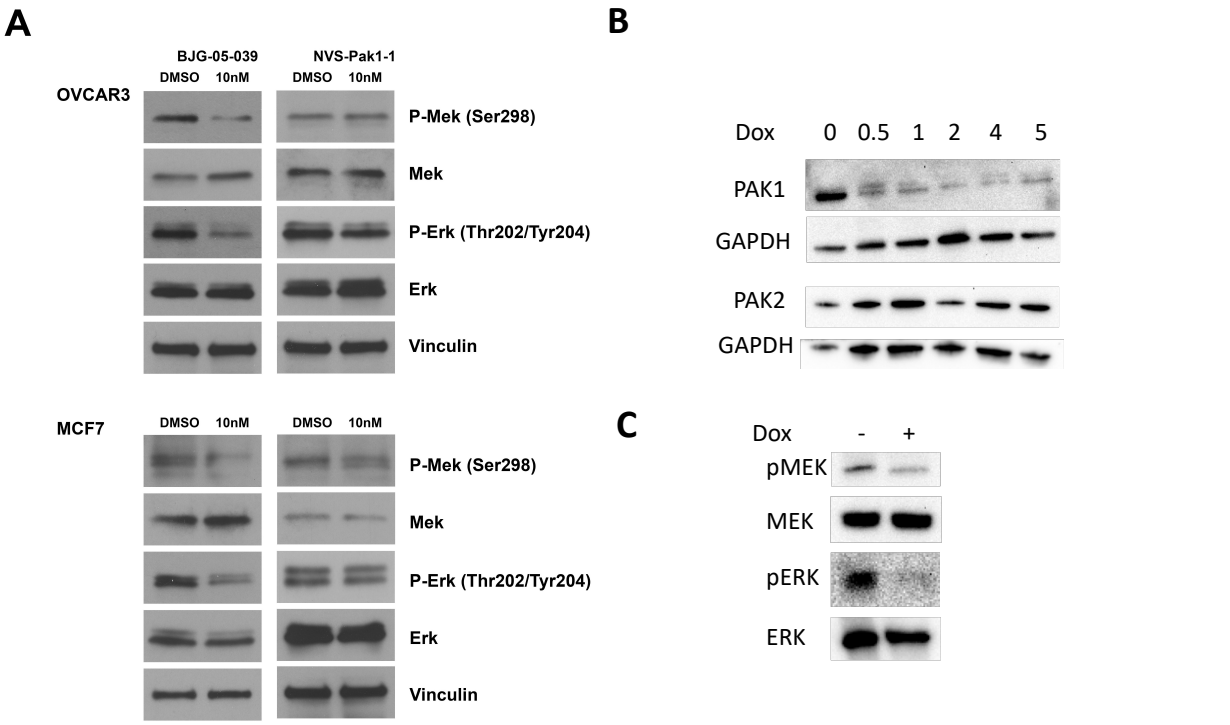

Chow et al Figure 3

Figure 3. PAK1 Degrader Potently Suppresses Proliferative Signals. A) OVCAR3 and MCF7 cells were treated for 24 h with DMSO, 10 nM BJG-05-039, or NVS-PAK1-1 as indicated. MEK and ERK phosphorylation was assessed by immunoblot with the indicated phosphorylation-specific antibodies. **B)** MCF7 cells were stably transduced with a doxycycline-regulated shRNA against PAK1 [27]. shRNA expression was induced by the indicated amounts of doxycycline (mg/ml) and immunoblots were performed using cell lysates 24 h post doxycycline addition. **C)** MCF7 cells were treated with vehicle or 1 mg/ml doxycycline. Immunoblots were performed using cell lysates 24 h post doxycycline addition.

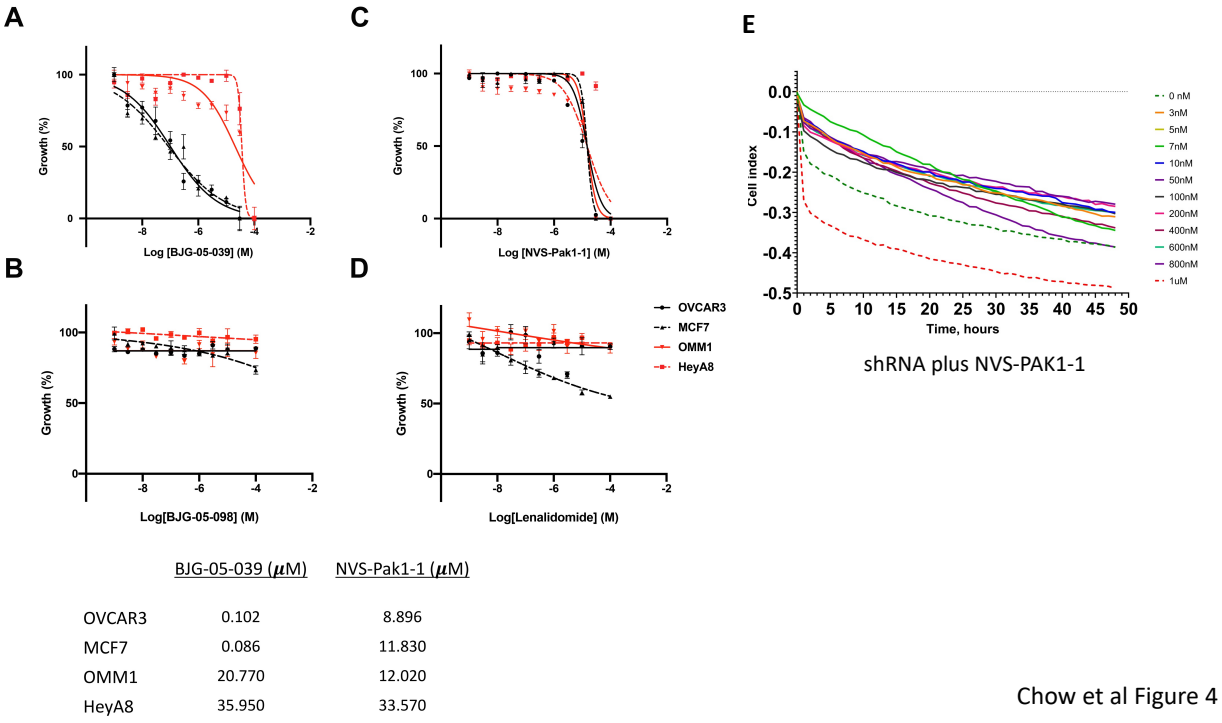

	BJG-05-039 (μM)	NVS-Pak1-1 (μM)
OVCAR3	0.102	8.896
MCF7	0.086	11.830
OMM1	20.770	12.020
HeyA8	35.950	33.570

Chow et al Figure 4

Figure 4. PAK1 Degrader Selectively Suppresses Proliferation of PAK1-Dependent Cells. PAK1-dependent (MCF7 and OVCAR3) and PAK2-dependent (OMM1 and HeyA8) cells were treated for 96 h with varying concentrations of **A)** BJG-05-039, **B)** BJG-05-098, **C)** NVS-PAK1-1, or **D)** lenalidomide. Cell proliferation was assessed by MTT assay and EC50 values were determined. EC50 values are shown below the graphs. **E)** The effect of reducing PAK1 expression on the potency of NVS-PAK1-1 was assessed by treating control MCF7 cells or MCF7 cells in which PAK1 expression was reduced ~50% via induction of a PAK1-specific shRNA at 0.5 mg/ml doxycycline.

ASSOCIATED CONTENT

Supporting Information

Additional tables and figures illustrating PAK1/NVS-PAK1-1 interaction, profiles of NVS-based (allosteric) degraders, KinomeSCAN data, degrader effects on total proteome, and biochemical data. This material is available free of charge via the Internet at http://pubs.acs.org

AUTHOR INFORMATION

Corresponding Author

*E-mail: Jonathan.Chernoff@fccc.edu. Phone: (215) 728-5319. Fax: (215) 728-3616.

Author Contributions

J.C. and N.S.G conceived of the study. B.J.G., S.T., J.H, K.A.D, and E.S.F. designed and synthesized the compounds, profiled the degrader against the kinome, and/or carried out the proteomic analysis in MOLT4 cells. S.K., B.A., and R.D, performed the structural analysis shown in Figure 1. H.-Y.C., S.K, and G.A, designed and conducted the biological profiling of the degraders.

Notes

N.S.G. is a founder, science advisory board member (SAB) and equity holder in Syros, C4, Allorion, Jengu, B2S, Inception, EoCys, CobroVentures (advisor), GSK (advisor), Larkspur (board member) and Soltego (board member). The Gray lab receives or has received research funding from Novartis, Takeda, Astellas, Taiho, Jansen, Kinogen, Arbella, Deerfield, Springworks, Interline and Sanofi. K.A.D is a consultant to Kronos Bio. E.S.F. is a founder, science advisory board member (SAB) and equity holder in Civetta Therapeutics, Jengu Therapeutics (board member) and Neomorph Inc. An advisor for EcoR1 capital, Deerfield, Sanofi and Avilar Therapeutics. The Fischer lab receives or has received research funding from Novartis, Astellas, Ajax, Voronoi, Interline and Deerfield.

ACKNOWLEDGMENTS

We thank Joachim Rudolph and Christopher Heise (Genentech) for data regarding the specificity of NVS-PAK1-1. This work was supported by grants from the NIH (J.C. CA227184 and CA148805; N.S.G and E.S.F. CA218278), and NCI Core Grant P30 CA06927 to FCCC.

ABBREVIATIONS USED

CDI, carbonyldiimidazole; CRBN, cereblon; DCM, dichloromethane; DIPEA, diisopropylethylamine; DMF, N,N-dimethylformamide; DMP, dess-martin periodane; DMSO, dimethyl sulfoxide; EtOAc, ethyl acetate; HATU, hexafluorophosphate azabenzotriazole tetramethyl uronium; HPLC, high-performance liquid chromatography; MeCN, acetonitrile; MeOH, methanol; MeI, methyl iodide, $Pd_2(dba)_3$, tris(dibenzylideneacetone)dipalladium(0);

PAK, p21-activated kinase; PROTAC, Proteolysis Targeting Chimera; TEA, triethylamine; TFA, trifluoroacetic acid; UPLC-MS, ultra-performance liquid chromatography-mass spectrometry; XPhos, 2-dicyclohexylphosphino-2′,4′,6′-triisopropylbiphenyl

REFERENCES

(1) Dummler, B.; Ohshiro, K.; Kumar, R.; Field, J. Pak protein kinases and their role in cancer. *Cancer metastasis reviews* **2009**, *28* (1-2), 51-63.
(2) Radu, M.; Semenova, G.; Kosoff, R.; Chernoff, J. Pak signaling during the development and progression of cancer. *Nat Rev Cancer.* **2014**, *14*, 13-25. DOI: 10.1038/nrc3645.
(3) Ye, D. Z.; Field, J. PAK signaling in cancer. *Cell Logist* **2012**, *2* (2), 105-116. DOI: 10.4161/cl.21882.
(4) Rane, C. K.; Minden, A. P21 activated kinase signaling in cancer. *Semin Cancer Biol* **2019**, *54*, 40-49. DOI: 10.1016/j.semcancer.2018.01.006.
(5) Jaffer, Z. M.; Chernoff, J. p21-activated kinases: three more join the Pak. *Int J Biochem Cell Biol* **2002**, *34* (7), 713-717, Comparative Study
Review. Rane, C. K.; Minden, A. P21 activated kinases: structure, regulation, and functions. *Small GTPases* **2014**, *5*. DOI: 10.4161/sgtp.28003.
(6) Sells, M. A.; Chernoff, J. Emerging from the Pak: the p21-activated protein kinase family. *Trends Cell Biol* **1997**, *7* (4), 162-167. DOI: 10.1016/S0962-8924(97)01003-9.
(7) Hofmann, C.; Shepelev, M.; Chernoff, J. The genetics of Pak. *J Cell Sci* **2004**, *117* (Pt 19), 4343-4354.
(8) Minden, A. PAK4-6 in cancer and neuronal development. *Cell Logist* **2012**, *2* (2), 95-104. DOI: 10.4161/cl.21171. Zhao, Z. S.; Manser, E. PAK family kinases: Physiological roles and regulation. *Cell Logist* **2012**, *2* (2), 59-68. DOI: 10.4161/cl.21912.
(9) Krauthammer, M.; Kong, Y.; Ha, B. H.; Evans, P.; Bacchiocchi, A.; McCusker, J. P.; Cheng, E.; Davis, M. J.; Goh, G.; Choi, M.; et al. Exome sequencing identifies recurrent somatic RAC1 mutations in melanoma. *Nature genetics* **2012**, *44* (9), 1006-1014. DOI: 10.1038/ng.2359. Araiza-Olivera, D.; Feng, Y.; Semenova, G.; Prudnikova, T. Y.; Rhodes, J.; Chernoff, J. Suppression of RAC1-driven malignant melanoma by group A PAK inhibitors. *Oncogene* **2018**, *37* (7), 944-952. DOI: 10.1038/onc.2017.400.
(10) Murray, B. W.; Guo, C.; Piraino, J.; Westwick, J. K.; Zhang, C.; Lamerdin, J.; Dagostino, E.; Knighton, D.; Loi, C. M.; Zager, M.; et al. Small-molecule p21-activated kinase inhibitor PF-3758309 is a potent inhibitor of oncogenic signaling and tumor growth. *Proc Natl Acad Sci U S A* **2010**, 9446-9451.
(11) Licciulli, S.; Maksimoska, J.; Zhou, C.; Troutman, S.; Kota, S.; Liu, Q.; Duron, S.; Campbell, D.; Chernoff, J.; Field, J.; et al. FRAX597, a small molecule inhibitor of the p21-activated kinases, inhibits tumorigenesis of neurofibromatosis type 2 (NF2)-associated Schwannomas. *J Biol Chem* **2013**, *288* (40), 29105-29114. DOI: 10.1074/jbc.M113.510933.
(12) Ong, C. C.; Gierke, S.; Pitt, C.; Sagolla, M.; Cheng, C. K.; Zhou, W.; Jubb, A. M.; Strickland, L.; Schmidt, M.; Duron, S. G.; et al. Small molecule inhibition of group I p21-activated kinases in breast cancer induces apoptosis and potentiates the activity of microtubule stabilizing agents. *Breast cancer research : BCR* **2015**, *17*, 59. DOI: 10.1186/s13058-015-0564-5.
(13) Ndubaku, C. O.; Crawford, J. J.; Drobnick, J.; Aliagas, I.; Campbell, D.; Dong, P.; Dornan, L. M.; Duron, S.; Epler, J.; Gazzard, L.; et al. Design of Selective PAK1 Inhibitor G-5555:

Improving Properties by Employing an Unorthodox Low-pK a Polar Moiety. *ACS Med Chem Lett* **2015**, *6* (12), 1241-1246. DOI: 10.1021/acsmedchemlett.5b00398.
(14) Rudolph, J.; Murray, L. J.; Ndubaku, C. O.; O'Brien, T.; Blackwood, E.; Wang, W.; Aliagas, I.; Gazzard, L.; Crawford, J. J.; Drobnick, J.; et al. Chemically Diverse Group I p21-Activated Kinase (PAK) Inhibitors Impart Acute Cardiovascular Toxicity with a Narrow Therapeutic Window. *J Med Chem* **2016**, *59* (11), 5520-5541. DOI: 10.1021/acs.jmedchem.6b00638.
(15) Chow, H. Y.; Jubb, A. M.; Koch, J. N.; Jaffer, Z. M.; Stepanova, D.; Campbell, D. A.; Duron, S. G.; O'Farrell, M.; Cai, K. Q.; Klein-Szanto, A. J.; et al. p21-Activated kinase 1 is required for efficient tumor formation and progression in a Ras-mediated skin cancer model. *Cancer Res* **2012**, *72* (22), 5966-5975. DOI: 0008-5472.CAN-12-2246 [pii] 10.1158/0008-5472.CAN-12-2246.
(16) Chow, H. Y.; Dong, B.; Duron, S. G.; Campbell, D. A.; Ong, C. C.; Hoeflich, K. P.; Chang, L. S.; Welling, D. B.; Yang, Z. J.; Chernoff, J. Group I Paks as therapeutic targets in NF2-deficient meningioma. *Oncotarget* **2015**, *6* (4), 1981-1994.
(17) Arias-Romero, L. E.; Villamar-Cruz, O.; Huang, M.; Hoeflich, K. P.; Chernoff, J. Pak1 Kinase Links ErbB2 to beta-Catenin in Transformation of Breast Epithelial Cells. *Cancer Res* **2013**, *73* (12), 3671-3682. DOI: 10.1158/0008-5472.CAN-12-4453.
(18) Radu, M.; Lyle, K.; Hoeflich, K. P.; Villamar-Cruz, O.; Koeppen, H.; Chernoff, J. p21-Activated Kinase 2 Regulates Endothelial Development and Function through the Bmk1/Erk5 Pathway. *Mol Cell Biol* **2015**, *35* (23), 3990-4005. DOI: 10.1128/MCB.00630-15.
(19) Allen, J. D.; Jaffer, Z. M.; Park, S. J.; Burgin, S.; Hofmann, C.; Sells, M. A.; Chen, S.; Derr-Yellin, E.; Michels, E. G.; McDaniel, A.; et al. p21-activated kinase regulates mast cell degranulation via effects on calcium mobilization and cytoskeletal dynamics. *Blood* **2009**, *113* (12), 2695-2705, Research Support, N.I.H., Extramural
Research Support, U.S. Gov't, Non-P.H.S. DOI: 10.1182/blood-2008-06-160861. Kelly, M. L.; Chernoff, J. Mouse models of PAK function. *Cell Logist* **2012**, *2* (2), 84-88. DOI: 10.4161/cl.21381.
(20) Karpov, A. S.; Amiri, P.; Bellamacina, C.; Bellance, M. H.; Breitenstein, W.; Daniel, D.; Denay, R.; Fabbro, D.; Fernandez, C.; Galuba, I.; et al. Optimization of a Dibenzodiazepine Hit to a Potent and Selective Allosteric PAK1 Inhibitor. *ACS Med Chem Lett* **2015**, *6* (7), 776-781. DOI: 10.1021/acsmedchemlett.5b00102.
(21) Hawley, E.; Gehlhausen, J.; Karchugina, S.; Chow, H.-Y.; Araiza-Olivera, D.; Radu, M.; Smith, A.; Burks, C.; Jiang, L.; Li, X.; et al. PAK1 inhibition reduces tumor size and extends the lifespan of mice in a genetically engineered mouse model of Neurofibromatosis Type 2 (NF2). *Human Mol. Genet.* **2021**.
(22) Kim, D. J.; Choi, C. K.; Lee, C. S.; Park, M. H.; Tian, X.; Kim, N. D.; Lee, K. I.; Choi, J. K.; Ahn, J. H.; Shin, E. Y.; et al. Small molecules that allosterically inhibit p21-activated kinase activity by binding to the regulatory p21-binding domain. *Exp Mol Med* **2016**, *48*, e229. DOI: 10.1038/emm.2016.13.
(23) Sells, M. A.; Knaus, U. G.; Bagrodia, S.; Ambrose, D. M.; Bokoch, G. M.; Chernoff, J. Human p21-activated kinase (Pak1) regulates actin organization in mammalian cells. *Curr Biol* **1997**, *7* (3), 202-210.
(24) Alessi, D. R.; Cuenda, A.; Cohen, P.; Dudley, D. T.; Saltiel, A. R. PD 098059 is a specific inhibitor of the activation of mitogen-activated protein kinase kinase in vitro and in vivo. *J Biol Chem* **1995**, *270* (46), 27489-27494. DOI: 10.1074/jbc.270.46.27489.

(25) Jia, Y.; Yun, C. H.; Park, E.; Ercan, D.; Manuia, M.; Juarez, J.; Xu, C.; Rhee, K.; Chen, T.; Zhang, H.; et al. Overcoming EGFR(T790M) and EGFR(C797S) resistance with mutant-selective allosteric inhibitors. *Nature* **2016**, *534* (7605), 129-132. DOI: 10.1038/nature17960.
(26) Shrestha, Y.; Schafer, E. J.; Boehm, J. S.; Thomas, S. R.; He, F.; Du, J.; Wang, S.; Barretina, J.; Weir, B. A.; Zhao, J. J.; et al. PAK1 is a breast cancer oncogene that coordinately activates MAPK and MET signaling. *Oncogene* **2012**, *31* (29), 3397-3408, Research Support, N.I.H., Extramural
Research Support, U.S. Gov't, Non-P.H.S. DOI: 10.1038/onc.2011.515.
(27) Prudnikova, T. Y.; Villamar-Cruz, O.; Rawat, S. J.; Cai, K. Q.; Chernoff, J. Effects of p21-activated kinase 1 inhibition on 11q13-amplified ovarian cancer cells. *Oncogene* **2016**, *35* (17), 2178-2185. DOI: 10.1038/onc.2015.278.
(28) An, S.; Fu, L. Small-molecule PROTACs: An emerging and promising approach for the development of targeted therapy drugs. *EBioMedicine* **2018**, *36*, 553-562. DOI: 10.1016/j.ebiom.2018.09.005.
(29) Brand, M.; Jiang, B.; Bauer, S.; Donovan, K. A.; Liang, Y.; Wang, E. S.; Nowak, R. P.; Yuan, J. C.; Zhang, T.; Kwiatkowski, N.; et al. Homolog-Selective Degradation as a Strategy to Probe the Function of CDK6 in AML. *Cell Chem Biol* **2019**, *26* (2), 300-306 e309. DOI: 10.1016/j.chembiol.2018.11.006.
(30) Soucy, T. A.; Smith, P. G.; Rolfe, M. Targeting NEDD8-activated cullin-RING ligases for the treatment of cancer. *Clinical cancer research : an official journal of the American Association for Cancer Research* **2009**, *15* (12), 3912-3916. DOI: 10.1158/1078-0432.CCR-09-0343.
(31) Donovan, K. A.; An, J.; Nowak, R. P.; Yuan, J. C.; Fink, E. C.; Berry, B. C.; Ebert, B. L.; Fischer, E. S. Thalidomide promotes degradation of SALL4, a transcription factor implicated in Duane Radial Ray syndrome. *Elife* **2018**, *7*. DOI: 10.7554/eLife.38430.
(32) Kronke, J.; Hurst, S. N.; Ebert, B. L. Lenalidomide induces degradation of IKZF1 and IKZF3. *Oncoimmunology* **2014**, *3* (7), e941742. DOI: 10.4161/21624011.2014.941742. Kronke, J.; Fink, E. C.; Hollenbach, P. W.; MacBeth, K. J.; Hurst, S. N.; Udeshi, N. D.; Chamberlain, P. P.; Mani, D. R.; Man, H. W.; Gandhi, A. K.; et al. Lenalidomide induces ubiquitination and degradation of CK1alpha in del(5q) MDS. *Nature* **2015**, *523* (7559), 183-188. DOI: 10.1038/nature14610.
(33) England, C. G.; Ehlerding, E. B.; Cai, W. NanoLuc: A Small Luciferase Is Brightening Up the Field of Bioluminescence. *Bioconjug Chem* **2016**, *27* (5), 1175-1187. DOI: 10.1021/acs.bioconjchem.6b00112.
(34) Slack-Davis, J. K.; Eblen, S. T.; Zecevic, M.; Boerner, S. A.; Tarcsafalvi, A.; Diaz, H. B.; Marshall, M. S.; Weber, M. J.; Parsons, J. T.; Catling, A. D. PAK1 phosphorylation of MEK1 regulates fibronectin-stimulated MAPK activation. *J Cell Biol* **2003**, *162*, 281-291. Coles, L. C.; Shaw, P. E. PAK1 primes MEK1 for phosphorylation by Raf-1 kinase during cross-cascade activation of the ERK pathway. *Oncogene* **2002**, *21* (14), 2236-2244. DOI: 10.1038/sj.onc.1205302.
(35) Semenova, G.; Chernoff, J. Targeting PAK1. *Biochemical Society transactions* **2017**, *45* (1), 79-88. DOI: 10.1042/BST20160134. Ong, C. C.; Jubb, A. M.; Jakubiak, D.; Zhou, W.; Rudolph, J.; Haverty, P. M.; Kowanetz, M.; Yan, Y.; Tremayne, J.; Lisle, R.; et al. P21-activated kinase 1 (PAK1) as a therapeutic target in BRAF wild-type melanoma. *J Natl Cancer Inst* **2013**, *105* (9), 606-607, Research Support, Non-U.S. Gov't. DOI: 10.1093/jnci/djt054. Liu, H.; Liu, K.; Dong, Z. The Role of p21-Activated Kinases in Cancer and Beyond: Where Are We Heading? *Front*

Cell Dev Biol **2021**, *9*, 641381. DOI: 10.3389/fcell.2021.641381. Senapedis, W.; Crochiere, M.; Baloglu, E.; Landesman, Y. Therapeutic Potential of Targeting PAK Signaling. *Anticancer Agents Med Chem* **2016**, *16* (1), 75-88. DOI: 10.2174/1871520615666150617111414. Rudolph, J.; Crawford, J. J.; Hoeflich, K. P.; Wang, W. Inhibitors of p21-activated kinases (PAKs). *J Med Chem* **2015**, *58* (1), 111-129. DOI: 10.1021/jm501613q.
(36) Uribe-Alvarez, C.; Guerrero-Rodriguez, S. L.; Rhodes, J.; Cannon, A.; Chernoff, J.; Araiza-Olivera, D. Targeting effector pathways in RAC1(P29S)-driven malignant melanoma. *Small GTPases* **2020**, 1-9. DOI: 10.1080/21541248.2020.1728469. Qasim, S. L.; Sierra, L.; Shuck, R.; Kurenbekova, L.; Patel, T. D.; Rajapakshe, K.; Wulff, J.; Nakahata, K.; Kim, H. R.; Landesman, Y.; et al. p21-activated kinases as viable therapeutic targets for the treatment of high-risk Ewing sarcoma. *Oncogene* **2021**, *40* (6), 1176-1190. DOI: 10.1038/s41388-020-01600-9. Knippler, C. M.; Saji, M.; Rajan, N.; Porter, K.; La Perle, K. M. D.; Ringel, M. D. MAPK- and AKT-activated thyroid cancers are sensitive to group I PAK inhibition. *Endocr Relat Cancer* **2019**, *26* (8), 699-712. DOI: 10.1530/ERC-19-0188. Semenova, G.; Stepanova, D. S.; Dubyk, C.; Handorf, E.; Deyev, S. M.; Lazar, A. J.; Chernoff, J. Targeting group I p21-activated kinases to control malignant peripheral nerve sheath tumor growth and metastasis. *Oncogene* **2017**, *36* (38), 5421-5431. DOI: 10.1038/onc.2017.143.
(37) Wang, S.; Bian, W.; Zhen, J.; Zhao, L.; Chen, W. Melatonin-Mediated Pak2 Activation Reduces Cardiomyocyte Death Through Suppressing Hypoxia Reoxygenation Injury-Induced Endoplasmic Reticulum Stress. *J Cardiovasc Pharmacol* **2019**, *74* (1), 20-29. DOI: 10.1097/FJC.0000000000000678. Binder, P.; Wang, S.; Radu, M.; Zin, M.; Collins, L.; Khan, S.; Li, Y.; Sekeres, K.; Humphreys, N.; Swanton, E.; et al. Pak2 as a Novel Therapeutic Target for Cardioprotective Endoplasmic Reticulum Stress Response. *Circulation research* **2019**, *124* (5), 696-711. DOI: 10.1161/CIRCRESAHA.118.312829.
(38) Cromm, P. M.; Samarasinghe, K. T. G.; Hines, J.; Crews, C. M. Addressing Kinase-Independent Functions of Fak via PROTAC-Mediated Degradation. *J Am Chem Soc* **2018**, *140* (49), 17019-17026. DOI: 10.1021/jacs.8b08008.
(39) Higuchi, M.; Onishi, K.; Kikuchi, C.; Gotoh, Y. Scaffolding function of PAK in the PDK1-Akt pathway. *Nat Cell Biol* **2008**, *10* (11), 1356-1364. DOI: 10.1038/ncb1795.
(40) Budagyan, K.; Chernoff, J. A Facile Method to Engineer Mutant Kras Alleles in an Isogenic Cell Background. *Methods Mol Biol* **2021**, *2262*, 323-334. DOI: 10.1007/978-1-0716-1190-6_20.
(41) Team, R. C. *R: A language and environment for statistical computing. R Foundation for Statistical Computing,*; 2014.
(42) Ritchie, M. E.; Phipson, B.; Wu, D.; Hu, Y.; Law, C. W.; Shi, W.; Smyth, G. K. limma powers differential expression analyses for RNA-sequencing and microarray studies. *Nucleic Acids Res* **2015**, *43* (7), e47. DOI: 10.1093/nar/gkv007.

KEY RESOURCES TABLE

REAGENT or RESOURCE	SOURCE	IDENTIFIER
Antibodies		
Rabbit monoclonal anti PAK1	Cell Signaling Technology	Cat# 2602; 1:1000
Rabbit monoclonal anti PAK2	Cell Signaling Technology	Cat# 2608; 1:1000
Rabbit polyclonal anti phospho-PAK1/2/3 (S141)	Invitrogen	Cat# 44940G; 1:1000

Rabbit anti ERK1/2	Cell Signaling Technology	Cat# 4695; 1:2500
Rabbit anti phospho-ERK1/2 (T202/Y204)	Cell Signaling Technology	Cat# 9101; 1:2500
Rabbit anti MEK1/2	Cell Signaling Technology	Cat# 9122; 1:1000
Rabbit anti phospho-MEK1 (S298)	Cell Signaling Technology	Cat# 9128; 1:1000
Rabbit anti GAPDH	Cell Signaling Technology	Cat# 2118; 1:2500
Chemicals, Cloning Materials, Plasmids, Peptides, and Recombinant Proteins		
DMSO	Fisher	Cat# BP231-100
Bortezomib (PS-341)	Selleckchem	Cat# S1013
Lenalidomide (CC-5013)	Selleckchem	Cat# S1029
NVS-PAK1-1	Sigma-Aldrich	Cat# SML1867
Valspodar	Sigma-Aldrich	Cat# SML0572
DMEM Medium	Gibco	Cat# 10566-016
RPMI Medium	Gibco	Cat# 72400-047
Fetal Bovine Serum	HyClone	Cat# SH30071.03
Penicillin Streptomycin	Gibco	Cat# 15150-122
PAK1 Protein	This study	NA
PAK2 Protein	This study	NA
Doxycycline Hyclate	Sigma-Aldrich	Cat# D9891-1G
Viral Boost Reagent	Alstem	Cat# VB100
Lipofectamine™ 3000	Invitrogen	Cat# L3000001
Lipofectamine™ RNAiMAX	Invitrogen	Cat# 13778100
ON-TARGETplus HUMAN PAK1 (5062) siRNA-SMARTpool	Dharmacon	Cat# L-003521-00-005
ON-TARGETplus HUMAN PAK2 (5058) siRNA-SMARTpool	Dharmacon	Cat# L-003597-00-0005
ON-TARGETplus Non-Targeting Pool	Dharmacon	Cat# D-001810-10-05
EcoRI restriction enzyme	NEB	Cat# R3101
XhoI restriction enzyme	NEB	Cat# R0146
In-Fusion HD Enzyme	Takara	Cat# 639649
Stellar competent cells	Takara	Cat# 636766
pFN31K-Nluc	Promega	Cat# N1321
pFN31K-Nluc-PAK1	This study	NA
pLenti-BFP	[40]	NA
pCMV6M-Pak1	Addgene	Cat# 12209
Nano-Glo® Endurazine™ Live Cell Substrate	Promega	Cat# N2570/1/2
Critical Commercial Assays		
Z-Lyte (PAK1)	Invitrogen	PV2830
Z-Lyte (PAK2)	Invitrogen	PV4565

Deposited Data		
BGY-05-039 Proteomics in MOLT4 cells	This study	Pride: PXccccc
Experimental Models: Cell Lines		
MOLT4	ATCC	CRL-1582; RRID: CVCL_0013
HEK293	ATCC	CRL-1573; RRID: CVCL_0031
OVCAR3	ATCC	HTB-161; RRID: CVCL_0465
MCF7	ATCC	HTB-22; RRID: CVCL_0031
HeyA8	MDACC	N/A
OMM1	Hans Grossniklaus, Emory University School of Medicine	N/A
Software and Algorithms		
GraphPad Prism	GraphPad Software, Inc.	www.graphpad.com/
Adobe Illustrator	Adobe Creative Cloud	https://www.adobe.com/creativecloud.html
Proteome Discoverer 2.2	Thermo Fisher Scientific	https://www.thermofisher.com/order/catalog/product/OPTION-30795
R Framework	Team RCR: A Language and Environment for Statistical Computing	http://www.R-project.org/
Python 3.7.3	Python Software Foundation	https://www.python.org/

LEAD CONTACT AND MATERIALS AVAILABILITY

Further information and request for resources and reagents should be directed to and will be fulfilled by the Lead Contact, Jonathan Chernoff (Jonathan.Chernoff@fccc.edu). Requested compounds will be provided following completion of an MTA.

Development and utility of a PAK1-selective degrader – Supplemental Information

Hoi-Yee Chow[1*], Sofiia Karchugina[1*], Brian J. Groendyke[2,4*], Sean Toenjes[5], John Hatcher[2], Katherine A. Donovan[2,3], Eric S. Fischer[2,3], Gleb Abalakov[1], Bulat Faezov[1], Roland Dunbrack[1], Nathanael S. Gray[5#], and Jonathan Chernoff[1,6#]

1 Fox Chase Cancer Center, Philadelphia, PA
2 Department of Cancer Biology; Dana Farber Cancer Institute, Boston, MA
3 Department of Biological Chemistry and Molecular Pharmacology, Harvard Medical School, Boston, MA
4 Current address: Blueprint Medicines, Cambridge, MA
5 Department of Chemical and Systems Biology, Chem-H and Stanford Cancer Institute, Stanford School of Medicine, Stanford University, Stanford, CA
6 Corresponding author: Jonathan Chernoff, Cancer Signaling and Epigenetics Program, Fox Chase Cancer Center, Philadelphia, Pennsylvania 19111, United States http://orcid.org/0000-0002-4803-7836; Email: Jonathan.Chernoff@fccc.edu

*These authors contributed equally to this work

Co-senior authors

Table of Contents

Figure S1. Surface representations of PAK1 and BJG-05-039 docked into the kinase. For clear demonstrations that the ligand occupies ATP pocket region of PAK1, S1A and S1B were taken from 90-degree apart angles. All figures were visualized in PyMOL 2.3.5

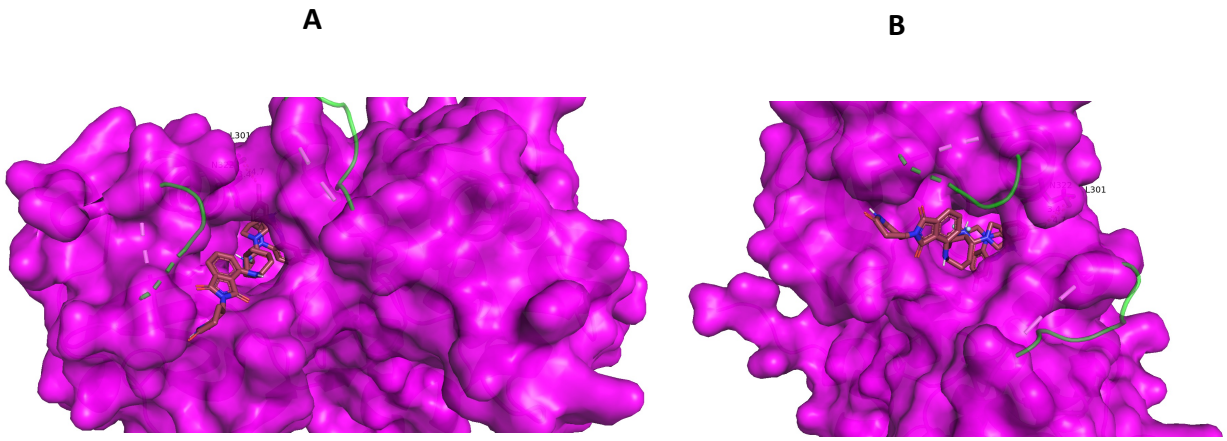

Chow et al Fig S1

Figure S2. A) Profiling NVS-based (allosteric) degraders BJG-05-014, BJG-05-027, and BJG-05-039 via western blots in Panc1 cells. Quantification is shown below. B) Profiling NVS-based (allosteric) degrader BJG-05-039 and ATP-competitive degraders BJG-05-093, BJG-05-094, and BJG-05-095 via western blots in Panc1 cells.

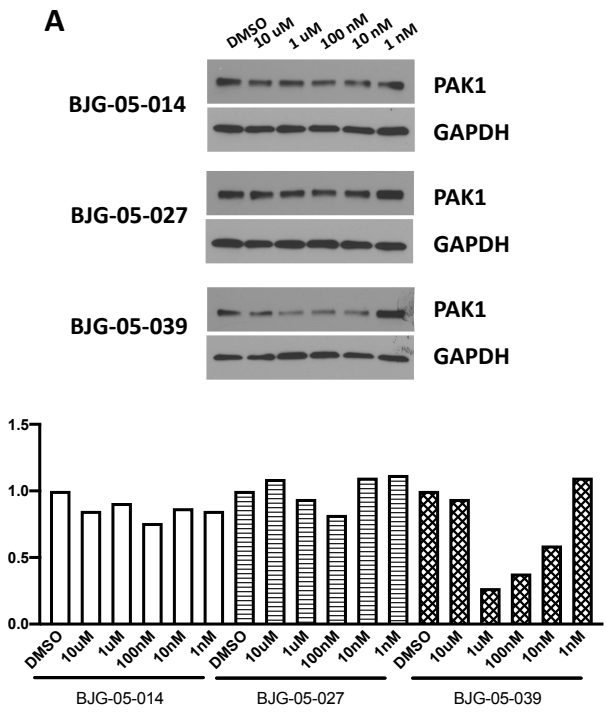

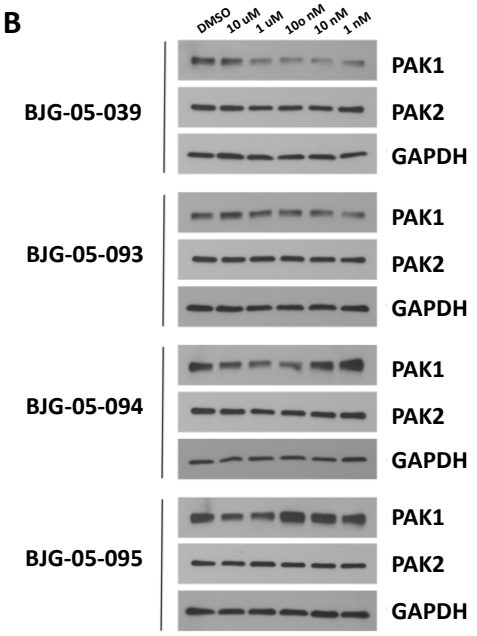

Chow et al Figure S2

Figure S3. KINOMEscan Profiling of BJG-05-039 @ 10μM. Image generated using TREEspot Software Tool and reprinted with permission from KINOMEscan, a division of DiscoveRx Corporation.

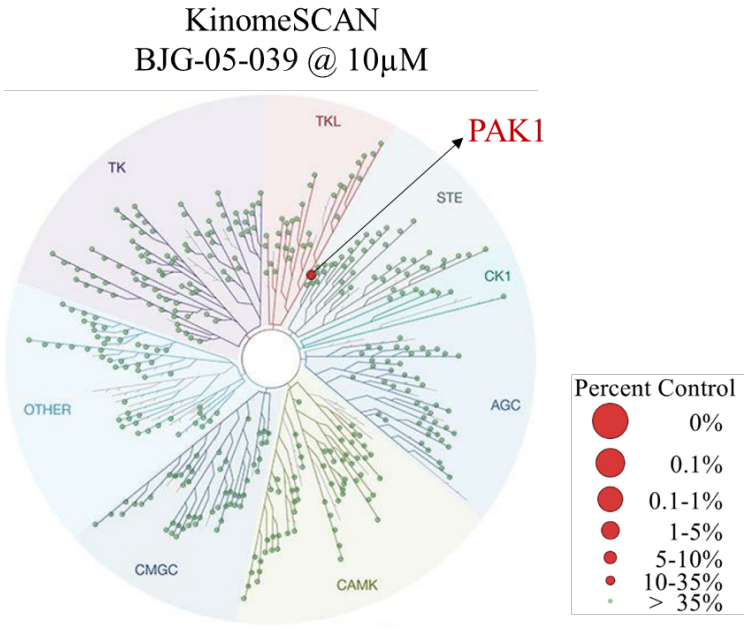

Figure S4. Effect of BJG-05-039 on Proteome. Scatterplot depicts the change in relative protein abundance of MOLT cells treated with BJG-05-039 (5 h, @ 1μM) compared with DMSO vehicle control-treated cells. Protein abundance measurements were made using tandem mass spectrometry and significant changes were assessed by moderated t test as implemented in the limma package (Ritchie et al., 2015). The log2 fold change (log2 FC) is shown on the y-axis and negative log10 p value (-log10 p value) on the x-axis for three independent biological replicates of each treatment.

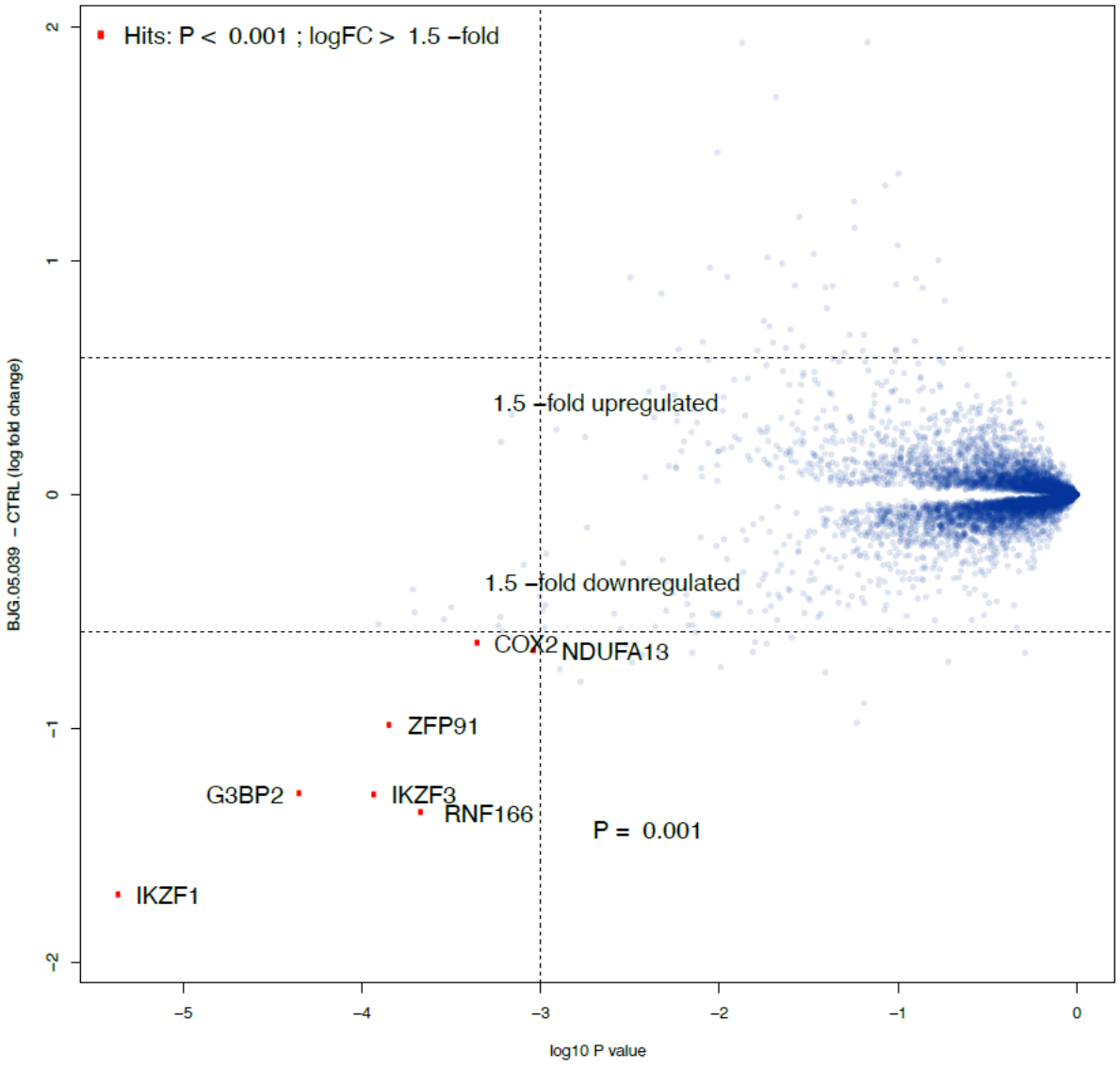

Table S1A. Biochemical IC_{50} data of allosteric PAK1 degraders.

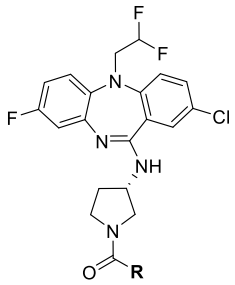

Compound	R	PAK1 IC_{50} (nM)	PAK2 IC_{50} (nM)	PAK4 IC_{50} (nM)
NVS-PAK-1		29.6	824	>10000
BJG-05-014	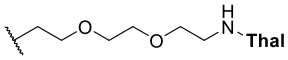	432	724	152
BJG-05-022	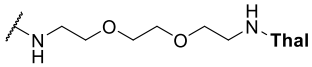	1490	6750	3860
BJG-05-019	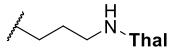	6300	>10000	>10000
BJG-05-017	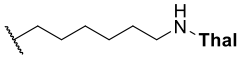	>1110	>3330	>1000
BJG-05-018	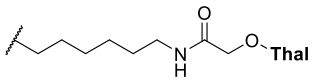	>3330	>10000	>10000
BJG-05-027	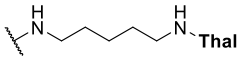	594	>10000	>10000
BJG-05-039	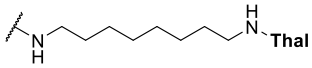	233	>10000	>10000
BJG-05-020	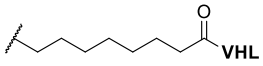	>10000	>10000	>10000
BJG-05-052	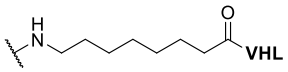	n/a	n/a	n/a
BJG-05-053	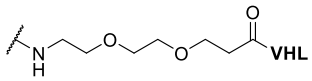	n/a	n/a	n/a
BJG-05-098	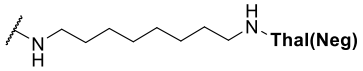	n/a	n/a	n/a
BJG-05-026	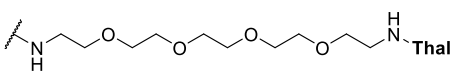	n/a	n/a	n/a

Table S1B. Biochemical IC_{50} data of ATP-competitive PAK1 degraders.

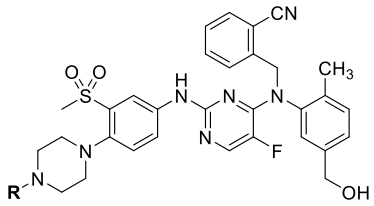

Compound	R	PAK1 IC_{50} (nM)	PAK2 IC_{50} (nM)	PAK4 IC_{50} (nM)
BJG-05-093	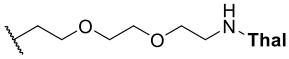	32.5	n/a	n/a
BJG-05-094	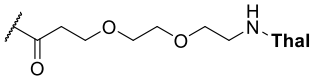	103	n/a	n/a
BJG-05-095	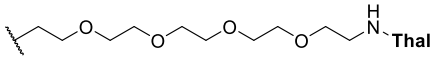	36.6	n/a	n/a

Table S2. KINOMEscan Profiling of BJG-05-039 @ 10μM.

BJG-05-039 @ 10μM		
DiscoveRx Gene Symbol	**Entrez Gene Symbol**	**Percent Control**
PAK1	PAK1	20
PRKD3	PRKD3	37
MARK2	MARK2	38
CAMK2A	CAMK2A	39
DAPK3	DAPK3	40
PHKG2	PHKG2	40
DAPK2	DAPK2	41
JAK1(JH1domain-catalytic)	JAK1	42
PAK7	PAK7	42
RPS6KA5(Kin.Dom.2-C-terminal)	RPS6KA5	42
WEE1	WEE1	42
ARK5	NUAK1	45
CAMK2D	CAMK2D	45
MAP4K4	MAP4K4	45
NDR2	STK38L	45
RSK4(Kin.Dom.2-C-terminal)	RPS6KA6	45
ACVR2B	ACVR2B	46
CAMK2B	CAMK2B	46

CAMKK2	CAMKK2	46
RET	RET	46
TLK1	TLK1	46
DAPK1	DAPK1	47
EPHA3	EPHA3	47
AAK1	AAK1	48
PRKX	PRKX	48
RSK1(Kin.Dom.2-C-terminal)	RPS6KA1	48
TNIK	TNIK	48
AXL	AXL	49
GSK3A	GSK3A	50
ACVR2A	ACVR2A	51
BRSK1	BRSK1	51
CAMK2G	CAMK2G	51
RSK3(Kin.Dom.2-C-terminal)	RPS6KA2	51
CAMK1	CAMK1	52
CAMKK1	CAMKK1	52
CSNK1G1	CSNK1G1	52
DDR1	DDR1	52
DMPK	DMPK	52
ERK4	MAPK4	52
MST3	STK24	52
NEK2	NEK2	52
CDC2L1	CDK11B	53
CDK9	CDK9	53
FLT3	FLT3	53
NLK	NLK	53
PRKD2	PRKD2	53
PKMYT1	PKMYT1	54
IRAK3	IRAK3	55
TTK	TTK	55
GAK	GAK	56
GCN2(Kin.Dom.2,S808G)	EIF2AK4	56
AKT3	AKT3	57
CHEK1	CHEK1	57
CLK1	CLK1	57
ERK5	MAPK7	57
PRKG1	PRKG1	57
DRAK2	STK17B	58
PCTK2	CDK17	58
DRAK1	STK17A	59
ERBB3	ERBB3	59
FLT3(K663Q)	FLT3	59

MAP4K5	MAP4K5	59
RET(V804M)	RET	59
RPS6KA4(Kin.Dom.1-N-terminal)	RPS6KA4	59
CSNK1D	CSNK1D	60
MAPKAPK2	MAPKAPK2	60
MUSK	MUSK	60
p38-alpha	MAPK14	60
PIK3CA	PIK3CA	60
CSNK1E	CSNK1E	61
MET(M1250T)	MET	61
CHEK2	CHEK2	62
CLK3	CLK3	62
PKAC-beta	PRKACB	62
STK16	STK16	62
TIE1	TIE1	62
ADCK4	ADCK4	63
CAMK1G	CAMK1G	63
CSNK1G3	CSNK1G3	63
ERK8	MAPK15	63
FLT3(D835Y)	FLT3	63
KIT(V559D,V654A)	KIT	63
MET(Y1235D)	MET	63
MRCKA	CDC42BPA	63
PIK3CA(H1047L)	PIK3CA	63
ERK3	MAPK6	64
FAK	PTK2	65
INSRR	INSRR	65
NEK5	NEK5	65
PHKG1	PHKG1	65
PKN2	PKN2	65
RIPK1	RIPK1	65
MLCK	MYLK3	66
EGFR(S752-I759del)	EGFR	67
FRK	FRK	67
HIPK4	HIPK4	67
MRCKB	CDC42BPB	67
MYO3A	MYO3A	67
RIPK2	RIPK2	67
TRKB	NTRK2	67
CAMK1D	CAMK1D	68
FGFR4	FGFR4	68
MET	MET	68
CDK2	CDK2	69

IGF1R	IGF1R	70
STK39	STK39	70
ACVRL1	ACVRL1	71
FYN	FYN	71
GRK4	GRK4	71
MAST1	MAST1	71
BRK	PTK6	72
DMPK2	CDC42BPG	72
LIMK2	LIMK2	72
MAP4K3	MAP4K3	72
PKNB(M.tuberculosis)	pknB	72
TRKA	NTRK1	72
TYRO3	TYRO3	72
YANK3	STK32C	72
ASK1	MAP3K5	73
BLK	BLK	73
BUB1	BUB1	73
TSSK1B	TSSK1B	73
BIKE	BMP2K	74
CAMK4	CAMK4	74
CDK3	CDK3	74
CSK	CSK	74
EGFR	EGFR	74
EGFR(L858R)	EGFR	74
EPHB2	EPHB2	74
MTOR	MTOR	74
WNK1	WNK1	74
PAK4	PAK4	75
PIM1	PIM1	75
STK33	STK33	75
TGFBR2	TGFBR2	75
FLT3(D835V)	FLT3	76
MAP3K2	MAP3K2	76
NIK	MAP3K14	76
SGK2	SGK2	76
ABL1(F317L)-nonphosphorylated	ABL1	77
CDKL2	CDKL2	77
DCAMKL1	DCLK1	77
FGFR2	FGFR2	77
GRK2	ADRBK1	77
PIK3CG	PIK3CG	77
PRKCQ	PRKCQ	77
WNK4	WNK4	77

ASK2	MAP3K6	78
CSNK1G2	CSNK1G2	78
CSNK2A2	CSNK2A2	78
EGFR(L747-E749del, A750P)	EGFR	78
PFTAIRE2	CDK15	78
PIK4CB	PI4KB	78
PIM3	PIM3	78
QSK	KIAA0999	78
ULK1	ULK1	78
WEE2	WEE2	78
DCAMKL3	DCLK3	79
LYN	LYN	79
NEK7	NEK7	79
PIKFYVE	PIKFYVE	79
YES	YES1	79
CDK8	CDK8	80
EGFR(L747-T751del,Sins)	EGFR	80
LRRK2	LRRK2	80
MST2	STK3	80
TLK2	TLK2	80
KIT(V559D)	KIT	81
MELK	MELK	81
PRKD1	PRKD1	81
PRKR	EIF2AK2	81
CDC2L5	CDK13	82
EGFR(L747-S752del, P753S)	EGFR	82
EPHA2	EPHA2	82
EPHA4	EPHA4	82
FGR	FGR	82
KIT	KIT	82
LZK	MAP3K13	82
NEK9	NEK9	82
PIM2	PIM2	82
PLK1	PLK1	82
RSK2(Kin.Dom.1-N-terminal)	RPS6KA3	82
SBK1	SBK1	82
STK36	STK36	82
TEC	TEC	82
TNNI3K	TNNI3K	82
ULK2	ULK2	82
ABL1-nonphosphorylated	ABL1	83
ADCK3	CABC1	83
AKT1	AKT1	83

AURKC	AURKC	83
CSNK1A1L	CSNK1A1L	83
EGFR(G719C)	EGFR	83
ERK1	MAPK3	83
FLT3(D835H)	FLT3	83
JNK1	MAPK8	83
MARK3	MARK3	83
MLK1	MAP3K9	83
NEK1	NEK1	83
SgK110	SgK110	83
STK35	STK35	83
TNK1	TNK1	83
YSK1	STK25	83
CDC2L2	CDC2L2	84
EGFR(G719S)	EGFR	84
EPHA8	EPHA8	84
FLT1	FLT1	84
JNK2	MAPK9	84
KIT(L576P)	KIT	84
LTK	LTK	84
RIOK1	RIOK1	84
RIOK3	RIOK3	84
ACVR1B	ACVR1B	85
BMPR1B	BMPR1B	85
CDK11	CDK19	85
ERK2	MAPK1	85
FGFR3	FGFR3	85
KIT(V559D,T670I)	KIT	85
MEK4	MAP2K4	85
PLK4	PLK4	85
PYK2	PTK2B	85
TAOK3	TAOK3	85
ABL1(T315I)-nonphosphorylated	ABL1	86
AKT2	AKT2	86
AMPK-alpha1	PRKAA1	86
CDK4	CDK4	86
DDR2	DDR2	86
EGFR(L858R,T790M)	EGFR	86
FES	FES	86
FLT4	FLT4	86
MEK6	MAP2K6	86
MST4	MST4	86
NDR1	STK38	86

PDGFRB	PDGFRB	86
PDPK1	PDPK1	86
ABL1(Q252H)-nonphosphorylated	ABL1	87
ANKK1	ANKK1	87
CAMK1B	PNCK	87
FLT3(ITD)	FLT3	87
KIT(D816V)	KIT	87
PAK2	PAK2	87
RIPK5	DSTYK	87
RSK1(Kin.Dom.1-N-terminal)	RPS6KA1	87
RSK2(Kin.Dom.2-C-terminal)	RPS6KA3	87
SRPK1	SRPK1	87
EGFR(L861Q)	EGFR	88
FER	FER	88
JNK3	MAPK10	88
MLK3	MAP3K11	88
MYO3B	MYO3B	88
PFTK1	CDK14	88
SGK3	SGK3	88
SRC	SRC	88
ACVR1	ACVR1	89
CSF1R	CSF1R	89
CTK	MATK	89
DYRK2	DYRK2	89
EPHB3	EPHB3	89
GRK1	GRK1	89
LKB1	STK11	89
MAP4K2	MAP4K2	89
NIM1	MGC42105	89
S6K1	RPS6KB1	89
SNRK	SNRK	89
WNK2	WNK2	89
WNK3	WNK3	89
BMX	BMX	90
CDK4-cyclinD1	CDK4	90
CDK5	CDK5	90
EPHA7	EPHA7	90
GSK3B	GSK3B	90
HASPIN	GSG2	90
HCK	HCK	90
MERTK	MERTK	90
MST1	STK4	90
PIK3C2B	PIK3C2B	90

PKAC-alpha	PRKACA	90
RET(M918T)	RET	90
RSK3(Kin.Dom.1-N-terminal)	RPS6KA2	90
TXK	TXK	90
ABL1(F317I)-nonphosphorylated	ABL1	91
EPHB4	EPHB4	91
IKK-alpha	CHUK	91
ITK	ITK	91
LCK	LCK	91
NEK6	NEK6	91
PCTK3	CDK18	91
PIK3CA(E542K)	PIK3CA	91
SLK	SLK	91
SRPK2	SRPK2	91
TYK2(JH1domain-catalytic)	TYK2	91
DCAMKL2	DCLK2	92
GRK3	ADRBK2	92
HPK1	MAP4K1	92
KIT(A829P)	KIT	92
p38-delta	MAPK13	92
SYK	SYK	92
TESK1	TESK1	92
TNK2	TNK2	92
ULK3	ULK3	92
AURKB	AURKB	93
CSNK1A1	CSNK1A1	93
ERN1	ERN1	93
INSR	INSR	93
MYLK2	MYLK2	93
SRPK3	SRPK3	93
TAOK2	TAOK2	93
YSK4	MAP3K19	93
ABL2	ABL2	94
CIT	CIT	94
EPHA6	EPHA6	94
FLT3(ITD,F691L)	FLT3	94
IKK-beta	IKBKB	94
LIMK1	LIMK1	94
MEK3	MAP2K3	94
MKNK2	MKNK2	94
PIK3CA(H1047Y)	PIK3CA	94
PRKCH	PRKCH	94
ROS1	ROS1	94

RPS6KA5(Kin.Dom.1-N-terminal)	RPS6KA5	94
TRPM6	TRPM6	94
VRK2	VRK2	94
CLK2	CLK2	95
FGFR3(G697C)	FGFR3	95
FLT3(ITD,D835V)	FLT3	95
MAP3K4	MAP3K4	95
PIK3C2G	PIK3C2G	95
PIP5K1A	PIP5K1A	95
PKN1	PKN1	95
RSK4(Kin.Dom.1-N-terminal)	RPS6KA6	95
SIK	SIK1	95
TAOK1	TAOK1	95
CSNK2A1	CSNK2A1	96
LRRK2(G2019S)	LRRK2	96
MEK2	MAP2K2	96
PIP5K1C	PIP5K1C	96
SNARK	NUAK2	96
ALK	ALK	97
EGFR(T790M)	EGFR	97
EPHB6	EPHB6	97
ERBB4	ERBB4	97
FGFR1	FGFR1	97
JAK3(JH1domain-catalytic)	JAK3	97
MLK2	MAP3K10	97
MST1R	MST1R	97
p38-beta	MAPK11	97
PCTK1	CDK16	97
PRKCD	PRKCD	97
PRP4	PRPF4B	97
RAF1	RAF1	97
SIK2	SIK2	97
SRMS	SRMS	97
TYK2(JH2domain-pseudokinase)	TYK2	97
ZAK	ZAK	97
ABL1(H396P)-nonphosphorylated	ABL1	98
BMPR1A	BMPR1A	98
BRAF	BRAF	98
CDKL3	CDKL3	98
EIF2AK1	EIF2AK1	98
EPHA1	EPHA1	98
EPHB1	EPHB1	98
LOK	STK10	98

MAK	MAK	98
MARK1	MARK1	98
PFCDPK1(P.falciparum)	CDPK1	98
RIPK4	RIPK4	98
TIE2	TEK	98
BRSK2	BRSK2	99
CASK	CASK	99
CDKL1	CDKL1	99
EPHA5	EPHA5	99
ICK	ICK	99
JAK2(JH1domain-catalytic)	JAK2	99
MAP3K15	MAP3K15	99
NEK10	NEK10	99
NEK4	NEK4	99
p38-gamma	MAPK12	99
PAK6	PAK6	99
PLK3	PLK3	99
RET(V804L)	RET	99
RIOK2	RIOK2	99
RPS6KA4(Kin.Dom.2-C-terminal)	RPS6KA4	99
YANK2	STK32B	99
ABL1(E255K)-phosphorylated	ABL1	100
ABL1(F317I)-phosphorylated	ABL1	100
ABL1(F317L)-phosphorylated	ABL1	100
ABL1(H396P)-phosphorylated	ABL1	100
ABL1(M351T)-phosphorylated	ABL1	100
ABL1(Q252H)-phosphorylated	ABL1	100
ABL1(T315I)-phosphorylated	ABL1	100
ABL1(Y253F)-phosphorylated	ABL1	100
ABL1-phosphorylated	ABL1	100
ALK(C1156Y)	ALK	100
ALK(L1196M)	ALK	100
AMPK-alpha2	PRKAA2	100
AURKA	AURKA	100
BMPR2	BMPR2	100
BRAF(V600E)	BRAF	100
BTK	BTK	100
CDK4-cyclinD3	CDK4	100
CDK7	CDK7	100
CDKL5	CDKL5	100
CLK4	CLK4	100
CSF1R-autoinhibited	CSF1R	100
DLK	MAP3K12	100

DYRK1A	DYRK1A	100
DYRK1B	DYRK1B	100
EGFR(E746-A750del)	EGFR	100
ERBB2	ERBB2	100
FLT3(N841I)	FLT3	100
FLT3(R834Q)	FLT3	100
FLT3-autoinhibited	FLT3	100
GRK7	GRK7	100
HIPK1	HIPK1	100
HIPK2	HIPK2	100
HIPK3	HIPK3	100
HUNK	HUNK	100
IKK-epsilon	IKBKE	100
IRAK1	IRAK1	100
IRAK4	IRAK4	100
JAK1(JH2domain-pseudokinase)	JAK1	100
KIT(D816H)	KIT	100
KIT-autoinhibited	KIT	100
LATS1	LATS1	100
LATS2	LATS2	100
MAP3K1	MAP3K1	100
MAP3K3	MAP3K3	100
MAPKAPK5	MAPKAPK5	100
MARK4	MARK4	100
MEK1	MAP2K1	100
MEK5	MAP2K5	100
MINK	MINK1	100
MKK7	MAP2K7	100
MKNK1	MKNK1	100
MYLK	MYLK	100
MYLK4	MYLK4	100
NEK11	NEK11	100
NEK3	NEK3	100
OSR1	OXSR1	100
PAK3	PAK3	100
PDGFRA	PDGFRA	100
PFPK5(P.falciparum)	MAL13P1.279	100
PIK3CA(C420R)	PIK3CA	100
PIK3CA(E545A)	PIK3CA	100
PIK3CA(E545K)	PIK3CA	100
PIK3CA(I800L)	PIK3CA	100
PIK3CA(M1043I)	PIK3CA	100
PIK3CA(Q546K)	PIK3CA	100

PIK3CB	PIK3CB	100
PIK3CD	PIK3CD	100
PIP5K2B	PIP4K2B	100
PIP5K2C	PIP4K2C	100
PLK2	PLK2	100
PRKCE	PRKCE	100
PRKCI	PRKCI	100
PRKG2	PRKG2	100
ROCK1	ROCK1	100
ROCK2	ROCK2	100
SGK	SGK1	100
TAK1	MAP3K7	100
TBK1	TBK1	100
TGFBR1	TGFBR1	100
TRKC	NTRK3	100
TSSK3	TSSK3	100
VEGFR2	KDR	100
VPS34	PIK3C3	100
YANK1	STK32A	100
ZAP70	ZAP70	100

Table S3. Proteomic data of BJG-05-039 @ 10μM for 5 hours in MOLT4 cells.

(See attachment)

General Chemistry Methods

Analytical grade solvents and commercially available reagents were purchased from commercial sources and used directly without further purification unless otherwise stated. Thin-layer chromatography (TLC) was carried out on Merck 60 F_{254} precoated, glass silica plates which were visualized by ultraviolet light. Experiments were conducted under ambient conditions unless otherwise stated. ^{1}H-NMR, ^{13}C-NMR, and ^{19}F-NMR spectra were recorded at room temperature using a Bruker 500 (^{1}H-NMR at 500 MHz, ^{13}C-NMR at 125 MHz, and ^{19}F-NMR at 471 MHz). Chemical shifts are reported in ppm with reference to solvent signals [^{1}H-NMR: $CDCl_3$ (7.26 ppm), DMSO-d_6 (2.50 ppm); ^{13}C-NMR: $CDCl_3$ (77.16 ppm), DMSO-d_6 (39.52 ppm)]. Signal patterns are indicated as s, singlet; br s, broad singlet; d, doublet; t, triplet, q, quartet; p, pentet; and m, multiplet. Mass spectrometry (MS) analysis was obtained on a Waters Acquity UPLC-MS system using electrospray ionization (ESI) in positive ion mode, reporting the molecular ion $[M+H]^+$, $[M+Na]^+$, or a suitable fragment ion. Flash chromatography purification was conducted using an ISCO CombiFlash RF+ with RediSep Rf silica cartridges. Preparative reverse-phase HPLC purification was conducted using a Waters model 2545 pump and 2489 UV/Vis detector using SunFire Prep C18 5 μm columns (18x100 mm, 20 mL/min flow rate; 30x250 mm, 40 mL/min flow rate), and a gradient solvent system of water (0.035% TFA)/methanol (0.035% TFA) or water (0.035% TFA)/acetonitrile (0.035% TFA).

Experimental Procedures and Characterizations

General Synthetic Scheme

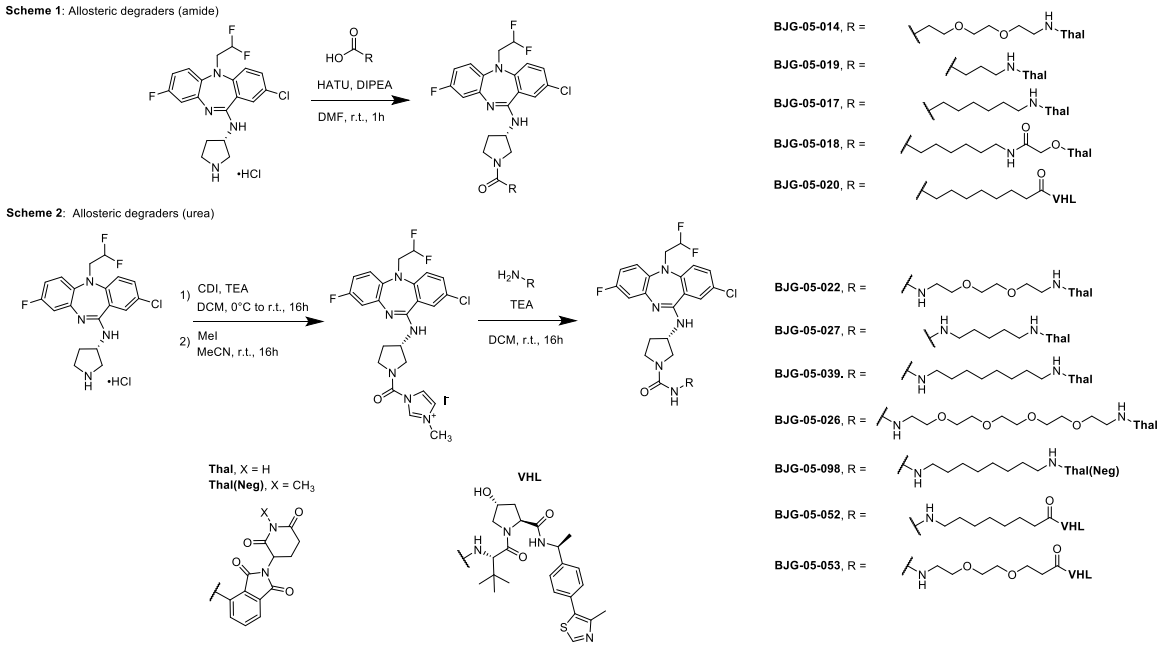

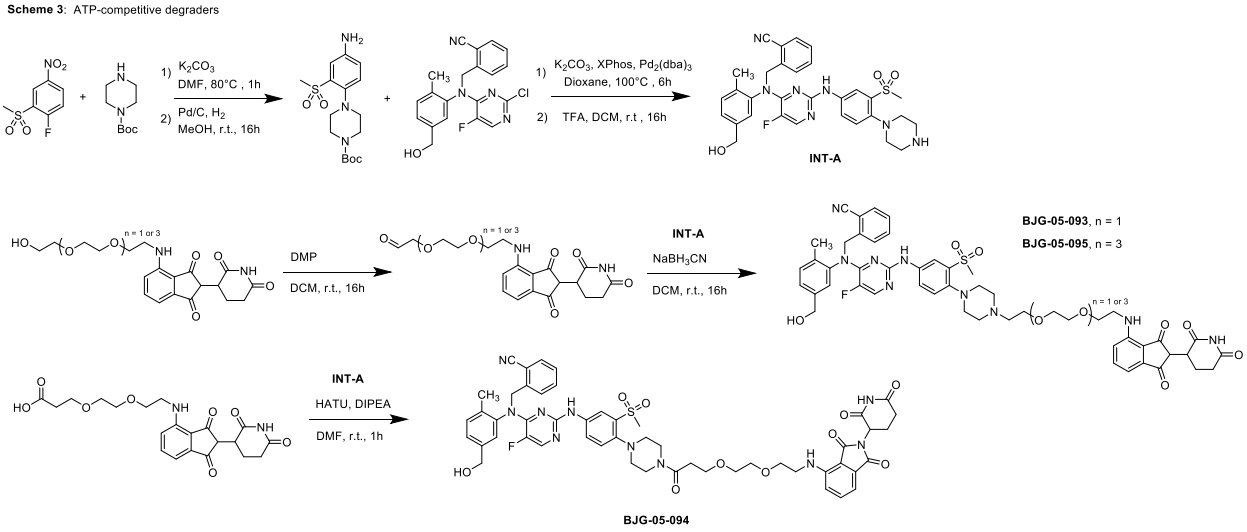

Synthetic Scheme 1: Allosteric degraders (amide exit vector)

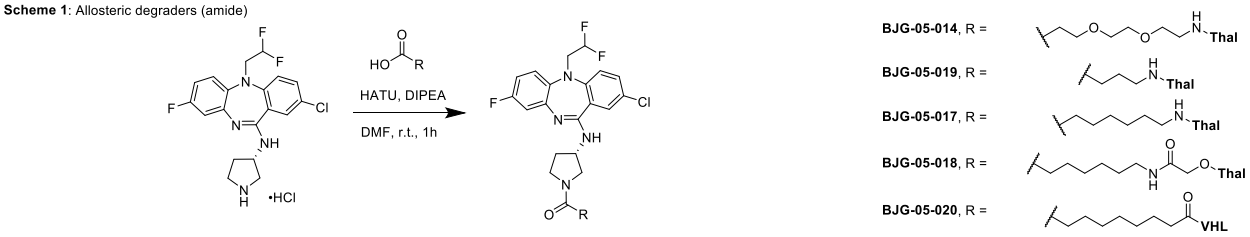

(S)-2-chloro-5-(2,2-difluoroethyl)-8-fluoro-N-(pyrrolidin-3-yl)-5H-dibenzo[b,e][1,4]diazepin-11-amine (HCl salt)

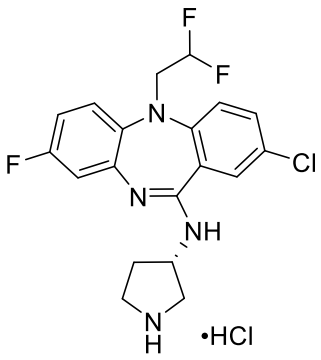

The compound was prepared according to the reported procedure.[1]

4-((2-(2-(3-((S)-3-((2-chloro-5-(2,2-difluoroethyl)-8-fluoro-5H-dibenzo[b,e][1,4]diazepin-11-yl)amino)pyrrolidin-1-yl)-3-oxopropoxy)ethoxy)ethyl)amino)-2-(2,6-dioxopiperidin-3-yl)isoindoline-1,3-dione **BJG-05-014**

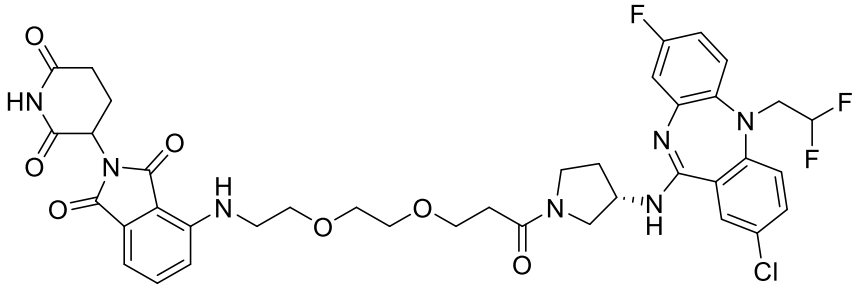

To a solution of solution of 3-(2-(2-((2-(2,6-dioxopiperidin-3-yl)-1,3-dioxoisoindolin-4-yl)amino)ethoxy)ethoxy)propanoic acid (13.0 mg, 0.030 mmol, 1 equv) in N, N-dimethylformamide (0.6 mL), disopropylamine (20.9 uL, 0.120 mmol, 4 equiv) and HATU (11.4 mg, 0.030 mmol, 1 equiv) were added. After stirring the mixture at room temperature for 5 minutes, (S)-2-chloro-5-(2,2-difluoroethyl)-8-fluoro-N-(pyrrolidin-3-yl)-5H-dibenzo[b,e][1,4]diazepin-11-amine (HCl salt) (12.9 mg, 0.030 mmol, 1 equiv) was added. After

2 hours of stirring, the reaction mixture was diluted with 1.0 mL of N, N-dimethylformamide and purified by reverse-phase prep HPLC (95-15% H_2O/MeOH, 40 mL/min, 45 min). Lyophilization from H_2O/MeCN provided the title compound as a yellow powder (3.8 mg, 16% yield TFA salt).

^{1}H NMR (500 MHz, DMSO-d_6) δ 11.09 (s, 1H), 7.79 – 7.39 (m, 4H), 7.32 (s, 1H), 7.14 (ddd, J = 9.6, 6.2, 3.8 Hz, 1H), 7.07 – 6.78 (m, 3H), 6.60 (t, J = 6.3 Hz, 1H), 6.03 (t, J = 55.8 Hz, 1H), 5.05 (dt, J = 12.8, 4.7 Hz, 1H), 4.71 – 4.52 (m, 1H), 4.23 (dd, J = 49.1, 14.0 Hz, 2H), 3.89 – 3.51 (m, 14H), 2.88 (td, J = 15.5, 14.2, 4.6 Hz, 1H), 2.63 – 2.52 (m, 2H), 2.35 – 2.09 (m, 1H), 2.07 – 1.94 (m, 2H). (Signals broadened due to rotational isomerism). LRMS (ESI) calculated for $[M+H]^+$ 810.26, found 809.71.

4-((7-((S)-3-((2-chloro-5-(2,2-difluoroethyl)-8-fluoro-5H-dibenzo[b,e][1,4]diazepin-11-yl)amino)pyrrolidin-1-yl)-7-oxoheptyl)amino)-2-(2,6-dioxopiperidin-3-yl)isoindoline-1,3-dione
BJG-05-017

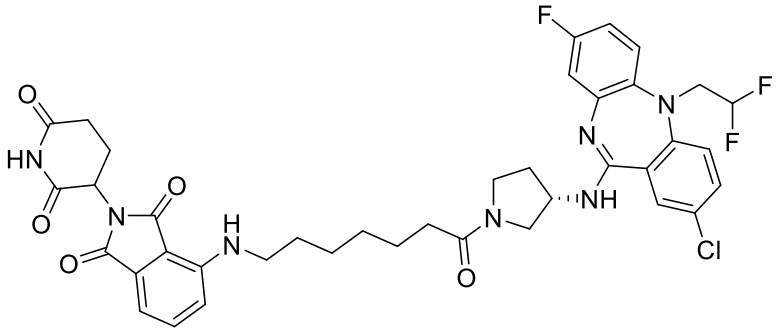

To a solution of solution of 7-((2-(2,6-dioxopiperidin-3-yl)-1,3-dioxoisoindolin-4-yl)amino)heptanoic acid (12.0 mg, 0.030 mmol, 1 equv) in N, N-dimethylformamide (0.6 mL), disopropylamine (20.9 uL, 0.120 mmol, 4 equiv) and HATU (11.4 mg, 0.030 mmol, 1 equiv) were added. After stirring the mixture at room temperature for 5 minutes, (S)-2-chloro-5-(2,2-difluoroethyl)-8-fluoro-N-(pyrrolidin-3-yl)-5H-dibenzo[b,e][1,4]diazepin-11-amine (HCl salt) (12.9 mg, 0.030 mmol, 1 equiv) was added. After 2 hours of stirring, the reaction mixture was diluted with 1.0 mL of N, N-dimethylformamide and purified by reverse-phase prep HPLC (95-15% H_2O/MeOH, 40 mL/min, 45 min). Lyophilization from H_2O/MeCN provided the title compound as a yellow powder (2.1 mg, 9% yield TFA salt).

^{1}H NMR (500 MHz, DMSO-d_6) δ 11.08 (s, 1H), 7.62 – 7.44 (m, 3H), 7.43 – 7.26 (m, 2H), 7.17 – 7.03 (m, 2H), 7.01 (d, J = 7.0 Hz, 1H), 6.77 – 6.61 (m, 2H), 6.52 (p, J = 6.0 Hz, 1H), 5.97 (tt, J = 55.7, 3.8 Hz, 1H), 5.11 – 4.98 (m, 1H), 4.63 – 4.46 (m, 1H), 4.25 – 3.98 (m, 2H), 3.75 – 3.59 (m, 1H), 3.58 – 3.34 (m, 5H), 2.88 (ddd, J = 17.4, 13.6, 5.4 Hz, 1H), 2.64 – 2.52 (m, 2H), 2.31 – 1.92 (m, 5H), 1.64 – 1.42 (m, 5H), 1.41 – 1.16 (m, 7H). 6:1 mix of rotamers. LRMS (ESI) calculated for $[M+H]^+$ 778.26, found 777.71.

N-(7-((S)-3-((2-chloro-5-(2,2-difluoroethyl)-8-fluoro-5H-dibenzo[b,e][1,4]diazepin-11-yl)amino)pyrrolidin-1-yl)-7-oxoheptyl)-2-((2-(2,6-dioxopiperidin-3-yl)-1,3-dioxoisoindolin-4-yl)oxy)acetamide **BJG-05-018**

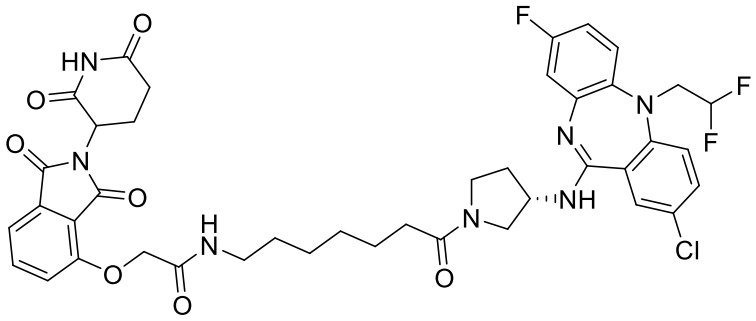

To a solution of solution of 7-(2-((2-(2,6-dioxopiperidin-3-yl)-1,3-dioxoisoindolin-4-yl)oxy)acetamido)heptanoic acid (13.8 mg, 0.030 mmol, 1 equv) in N, N-dimethylformamide (0.6 mL), disopropylamine (20.9 uL, 0.120 mmol, 4 equiv) and HATU (11.4 mg, 0.030 mmol, 1 equiv) were added. After stirring the mixture at room temperature for 5 minutes, (S)-2-chloro-5-(2,2-difluoroethyl)-8-fluoro-N-(pyrrolidin-3-yl)-5H-dibenzo[b,e][1,4]diazepin-11-amine (HCl salt) (12.9 mg, 0.030 mmol, 1 equiv) was added. After 2 hours of stirring, the reaction mixture was diluted with 1.0 mL of N, N-dimethylformamide and purified by reverse-phase prep HPLC (95-15% H_2O/MeOH, 40 mL/min, 45 min). Lyophilization from H_2O/MeCN provided the title compound as a yellow powder (2.5 mg, 10% yield TFA salt).

^{1}H NMR (500 MHz, DMSO-d_6) δ 11.11 (s, 1H), 7.97 – 7.88 (m, 1H), 7.85 – 7.78 (m, 1H), 7.61 – 7.46 (m, 3H), 7.42 – 7.28 (m, 3H), 7.11 (t, J = 7.7 Hz, 1H), 6.77 – 6.62 (m, 2H), 5.99 (tt, J = 55.1, 3.8 Hz, 1H), 5.12 (ddd, J = 12.6, 5.4, 2.2 Hz, 1H), 4.77 (s, 2H), 4.65 – 4.46 (m, 1H), 4.26 – 3.97 (m, 2H), 3.75 – 3.59 (m, 1H), 3.57 – 3.35 (m, 5H), 3.12 (dq, J = 13.2, 6.3 Hz, 2H), 2.90 (ddd, J = 19.0, 13.7, 5.4 Hz, 1H), 2.64 – 2.52 (m, 2H), 2.30 – 1.94 (m, 5H), 1.56 – 1.35 (m, 4H), 1.34 – 1.21 (m, 5H). LRMS (ESI) calculated for $[M+H]^+$ 836.27, found 835.61.

4-((4-((S)-3-((2-chloro-5-(2,2-difluoroethyl)-8-fluoro-5H-dibenzo[b,e][1,4]diazepin-11-yl)amino)pyrrolidin-1-yl)-4-oxobutyl)amino)-2-(2,6-dioxopiperidin-3-yl)isoindoline-1,3-dione **BJG-05-019**

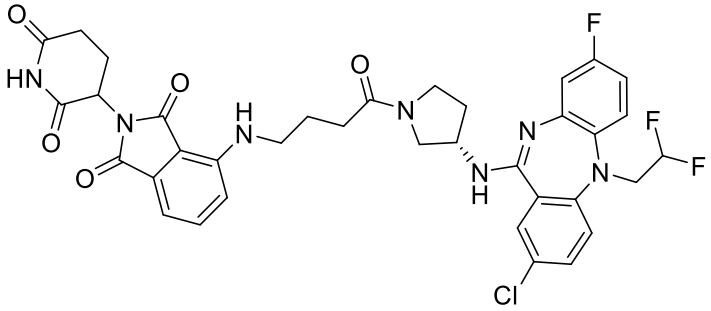

To a solution of solution of 4-((2-(2,6-dioxopiperidin-3-yl)-1,3-dioxoisoindolin-4-yl)amino)butanoic acid (14.4 mg, 0.040 mmol, 1 equv) in N, N-dimethylformamide (0.8 mL), disopropylamine (27.9 uL, 0.160 mmol, 4 equiv) and HATU (15.2 mg, 0.040 mmol, 1 equiv) were added. After stirring the mixture at room temperature for 5 minutes, (S)-2-chloro-5-(2,2-difluoroethyl)-8-fluoro-N-(pyrrolidin-3-yl)-5H-dibenzo[b,e][1,4]diazepin-11-amine (HCl salt) (17.2 mg, 0.040 mmol, 1 equiv) was added. After 2 hours of stirring, the reaction mixture was diluted with 1.0 mL of N, N-dimethylformamide and purified by reverse-phase prep HPLC (95-15% H_2O/MeOH, 40 mL/min, 45 min). Lyophilization from H_2O/MeCN provided the title compound as a yellow powder (4.1 mg, 14% yield TFA salt).

^{1}H NMR (500 MHz, DMSO-d_6) δ 11.09 (s, 1H), 7.80 – 7.29 (m, 5H), 7.23 – 7.15 (m, 1H), 7.14 – 6.97 (m, 2H), 6.68 (s, 1H), 6.09 (t, J = 55.0 Hz, 1H), 5.04 (dt, J = 12.9, 5.3 Hz, 1H), 4.65 (d, J = 26.9 Hz, 1H), 4.41 – 4.12 (m, 2H), 3.41 – 3.28 (m, 2H), 2.96 – 2.78 (m, 1H), 2.64 – 2.52 (m, 2H), 2.44 – 1.96 (m, 5H), 1.90 – 1.74 (m, 2H). (Signals broadened due to rotational isomerism). LRMS (ESI) calculated for $[M+H]^+$ 736.21, found 735.71.

(2S,4R)-1-((S)-2-(9-((S)-3-((2-chloro-5-(2,2-difluoroethyl)-8-fluoro-5H-dibenzo[b,e][1,4]diazepin-11-yl)amino)pyrrolidin-1-yl)-9-oxononanamido)-3,3-dimethylbutanoyl)-4-hydroxy-N-((S)-1-(4-(4-methylthiazol-5-yl)phenyl)ethyl)pyrrolidine-2-carboxamide **BJG-05-020**

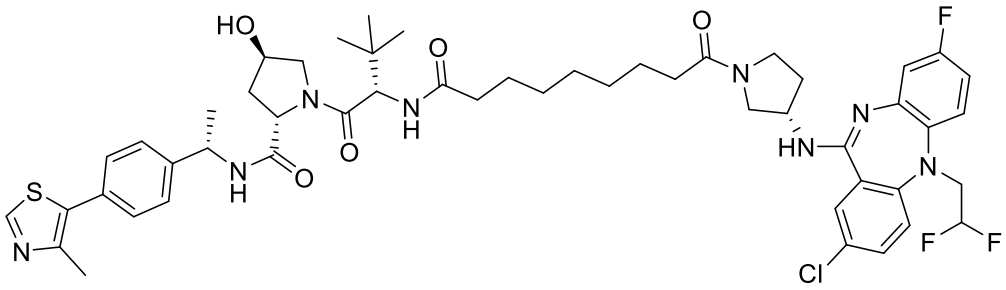

To a solution of solution of 9-(((S)-1-((2S,4R)-4-hydroxy-2-(((S)-1-(4-(4-methylthiazol-5-yl)phenyl)ethyl)carbamoyl)pyrrolidin-1-yl)-3,3-dimethyl-1-oxobutan-2-yl)amino)-9-oxononanoic acid (9.2 mg, 0.015 mmol, 1 equv) in N, N-dimethylformamide (0.3 mL), disopropylamine (10.5 uL, 0.060 mmol, 4 equiv) and HATU (5.7 mg, 0.015 mmol, 1 equiv) were added. After stirring the mixture at room temperature for 5 minutes, (S)-2-chloro-5-(2,2-difluoroethyl)-8-fluoro-N-(pyrrolidin-3-yl)-5H-dibenzo[b,e][1,4]diazepin-11-amine (HCl salt) (6.5 mg, 0.015 mmol, 1 equiv) was added. After 2 hours of stirring, the reaction mixture was diluted with 1.0 mL of N, N-dimethylformamide and purified by reverse-phase prep HPLC (95-5% H_2O/MeOH, 40 mL/min, 45 min). Lyophilization from H_2O/MeCN provided the title compound as a white powder (2.7 mg, 18% yield TFA salt).

^{1}H NMR (500 MHz, DMSO-d_6) δ 8.98 (s, 1H), 8.37 (d, J = 8.0 Hz, 1H), 7.77 (d, J = 9.1 Hz, 1H), 7.74 – 7.46 (m, 3H), 7.46 – 7.30 (m, 5H), 7.26 – 6.91 (m, 1H), 6.10 (t, J = 55.3 Hz, 1H), 4.91 (p, J = 7.0 Hz, 1H), 4.73 – 4.58 (m, 1H), 4.51 (dd, J = 9.3, 5.2 Hz, 1H), 4.42 (t, J = 8.1 Hz, 1H), 3.63 – 3.55 (m, 4H), 2.45 (s, 4H), 2.31 – 1.94 (m, 7H), 1.83 – 1.75 (m, 1H), 1.56 – 1.40 (m, 5H), 1.37 (d, J = 6.9 Hz, 3H), 1.32 – 1.16 (m, 7H), 0.93 (s, 9H). LRMS (ESI) calculated for $[M+H]^+$ 991.42, found 990.73.

Synthetic Scheme 2: Allosteric degraders (urea exit vector)

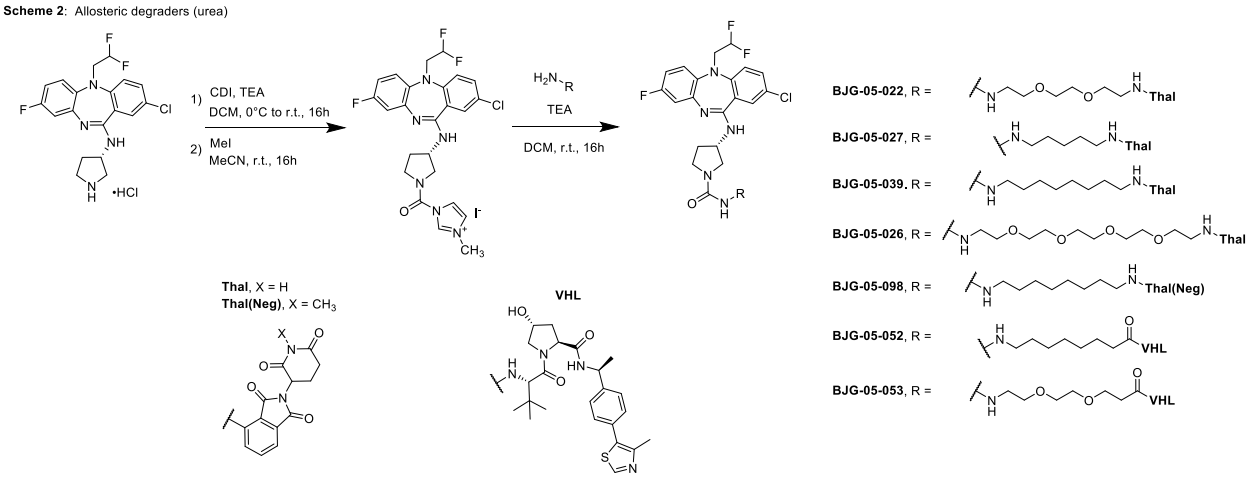

(S)-1-(3-((2-chloro-5-(2,2-difluoroethyl)-8-fluoro-5H-dibenzo[b,e][1,4]diazepin-11-yl)amino)pyrrolidine-1-carbonyl)-3-methyl-1H-imidazol-3-ium iodide

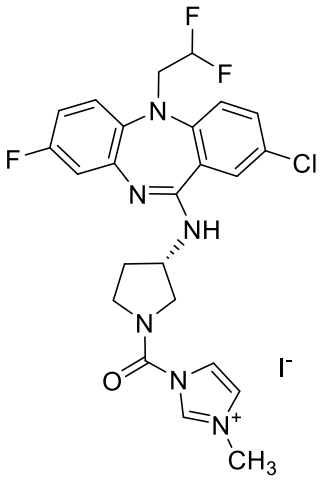

A solution of carbonyldiimidazole (50 mg, 0.31 mmol, 1.1 equiv) in dichloromethane (1.4 mL) was cooled to 0 °C at which (S)-2-chloro-5-(2,2-difluoroethyl)-8-fluoro-N-(pyrrolidin-3-yl)-5H-dibenzo[b,e][1,4]diazepin-11-amine (HCl salt) (120.8 mg, 0.28 mmol, 1.0 equiv) was added followed by addition of triethylamine (39 uL, 0.28 mmol, 1 equiv). The mixture was then removed from ice and allowed to stir at room temperature overnight. The reaction was diluted with 7 mL of water and organic layer was then extracted with dichloromethane (5x2 mL). The combined organic layers were washed with brine, dried over $MgSO_4$, filtered, and concentrated to provide a clear yellow oil (60 mg). Product was shown as the major component via mass spec: LRMS (ESI) calculated for $[M+H]^+$ 489.13, found 488.90. The crude product was moved forward without purification.

To a solution of 50 mg of crude residue in acetonitrile (1.4 mL), iodomethane (70 uL, 1.12 mmol, 4 equiv) was added at room temperature and stirred overnight. The reaction mixture was concentrated to provide the titled compound as a yellow oil (62.5 mg, 99% yield). The product

was shown as the major component via mass spec, LRMS (ESI) calculated for $[M+H]^+$ 504.16, found 502.78, and moved on to the next step without purification.

(3S)-3-((2-chloro-5-(2,2-difluoroethyl)-8-fluoro-5H-dibenzo[b,e][1,4]diazepin-11-yl)amino)-N-(2-(2-(2-((2-(2,6-dioxopiperidin-3-yl)-1,3-dioxoisoindolin-4-yl)amino)ethoxy)ethoxy)ethyl)pyrrolidine-1-carboxamide **BJG-05-022**

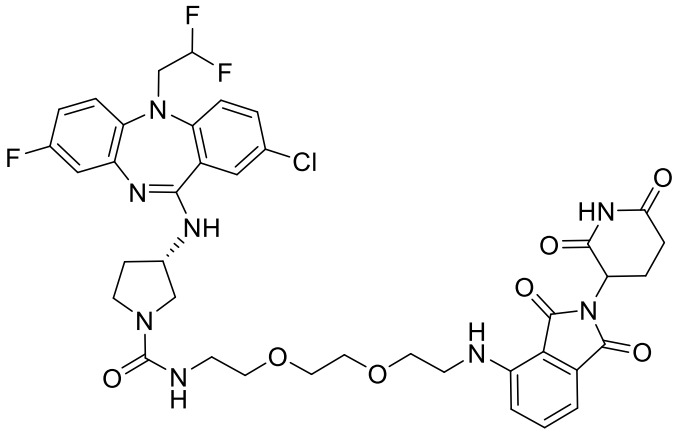

To a solution of solution of 4-((2-(2-(2-aminoethoxy)ethoxy)ethyl)amino)-2-(2,6-dioxopiperidin-3-yl)isoindoline-1,3-dione (15.6 mg, 0.030 mmol, 1 equiv) and (S)-1-(3-((2-chloro-5-(2,2-difluoroethyl)-8-fluoro-5H-dibenzo[b,e][1,4]diazepin-11-yl)amino)pyrrolidine-1-carbonyl)-3-methyl-1H-imidazol-3-ium iodide (18.9 mg, 0.030 mmol, 1 equv) in dichloromethane (0.3 mL), triethylamine (10.5 uL, 0.075 mmol, 2.5 equiv) was added. After 16 hours of stirring, the reaction mixture was rotovapped and diluted with 1.0 mL of N, N-dimethylformamide and purified by reverse-phase prep HPLC (95-15% H_2O/MeOH, 40 mL/min, 45 min). Lyophilization from H_2O/MeCN provided the title compound as a yellow powder (5.1 mg, 21% yield TFA salt).

^{1}H NMR (500 MHz, DMSO-d_6) δ 11.09 (s, 1H), 7.69 (s, 1H), 7.58 (ddd, J = 8.5, 7.0, 1.5 Hz, 2H), 7.49 (s, 1H), 7.39 (s, 1H), 7.27 – 6.98 (m, 4H), 6.60 (s, 1H), 6.33 – 5.89 (m, 2H), 5.06 (dd, J = 12.6, 5.4 Hz, 1H), 4.60 (s, 1H), 4.40 – 4.14 (m, 2H), 4.10 (d, J = 1.1 Hz, 1H), 3.57 – 3.29 (m, 12H), 3.18 (dq, J = 12.1, 6.1 Hz, 2H), 2.88 (ddd, J = 16.7, 13.6, 5.4 Hz, 1H), 2.62 – 2.52 (m, 2H), 2.34 – 1.95 (m, 3H). LRMS (ESI) calculated for $[M+H]^+$ 825.26, found 824.71.

(3S)-3-((2-chloro-5-(2,2-difluoroethyl)-8-fluoro-5H-dibenzo[b,e][1,4]diazepin-11-yl)amino)-N-(14-((2-(2,6-dioxopiperidin-3-yl)-1,3-dioxoisoindolin-4-yl)amino)-3,6,9,12-tetraoxatetradecyl)pyrrolidine-1-carboxamide **BJG-05-026**

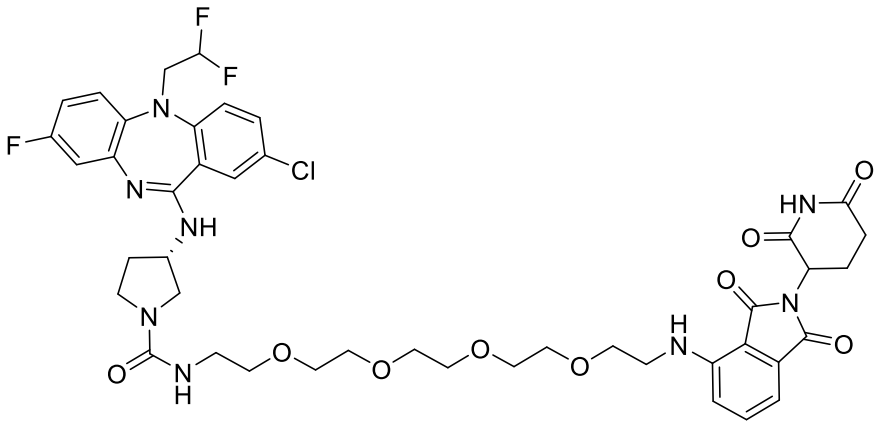

To a solution of solution of 4-((14-amino-3,6,9,12-tetraoxatetradecyl)amino)-2-(2,6-dioxopiperidin-3-yl)isoindoline-1,3-dione (23 mg, 0.030 mmol, 1 equiv) and (S)-1-(3-((2-chloro-5-(2,2-difluoroethyl)-8-fluoro-5H-dibenzo[b,e][1,4]diazepin-11-yl)amino)pyrrolidine-1-carbonyl)-3-methyl-1H-imidazol-3-ium iodide (18.9 mg, 0.030 mmol, 1 equv) in dichloromethane (0.3 mL), triethylamine (10.5 uL, 0.075 mmol, 2.5 equiv) was added. After 16 hours of stirring, the reaction mixture was rotovapped and diluted with 1.0 mL of N, N-dimethylformamide and purified by reverse-phase prep HPLC (95-15% H_2O/MeOH, 40 mL/min, 45 min). Lyophilization from H_2O/MeCN provided the title compound as a yellow powder (4.8 mg, 18% yield TFA salt).

^{1}H NMR (500 MHz, DMSO-d_6) δ 11.09 (s, 1H), 7.67 – 7.46 (m, 3H), 7.44 – 7.24 (m, 2H), 7.18 – 7.07 (m, 2H), 7.04 (d, J = 7.0 Hz, 1H), 6.79 – 6.63 (m, 2 H), 6.60 (t, J = 5.9 Hz, 1H), 6.21 – 5.82 (m, 2H), 5.05 (dd, J = 12.7, 5.5 Hz, 1H), 4.53 (t, J = 4.9 Hz, 1H), 4.28 – 3.93 (m, 2H), 3.64 – 3.34 (m, 20H), 3.24 – 3.10 (m, 2H), 2.88 (ddd, J = 16.7, 13.7, 5.4 Hz, 1H), 2.62 – 2.51 (m, 2H), 2.24 – 1.87 (m, 3H). LRMS (ESI) calculated for $[M+H]^+$ 913.31, found 912.62.

(3S)-3-((2-chloro-5-(2,2-difluoroethyl)-8-fluoro-5H-dibenzo[b,e][1,4]diazepin-11-yl)amino)-N-(5-((2-(2,6-dioxopiperidin-3-yl)-1,3-dioxoisoindolin-4-yl)amino)pentyl)pyrrolidine-1-carboxamide **BJG-05-027**

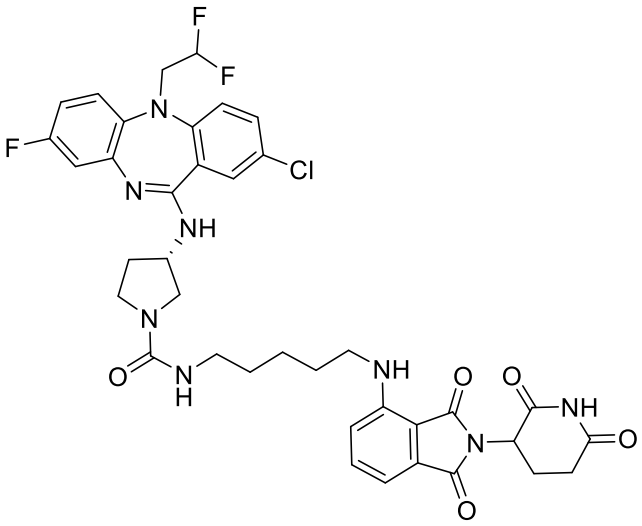

To a solution of solution of 4-((5-aminopentyl)amino)-2-(2,6-dioxopiperidin-3-yl)isoindoline-1,3-dione (15.1 mg, 0.030 mmol, 1 equiv) and (S)-1-(3-((2-chloro-5-(2,2-difluoroethyl)-8-fluoro-5H-dibenzo[b,e][1,4]diazepin-11-yl)amino)pyrrolidine-1-carbonyl)-3-methyl-1H-imidazol-3-ium iodide (18.9 mg, 0.030 mmol, 1 equv) in dichloromethane (0.3 mL), triethylamine (10.5 uL, 0.075 mmol, 2.5 equiv) was added. After 16 hours of stirring, the reaction mixture was rotovapped and diluted with 1.0 mL of N, N-dimethylformamide and purified by reverse-phase prep HPLC (95-15% H_2O/MeOH, 40 mL/min, 45 min). Lyophilization from H_2O/MeCN provided the title compound as a yellow powder (3.8 mg, 16% yield TFA salt).

^{1}H NMR (500 MHz, DMSO-d_6) δ 11.09 (s, 1H), 7.70 (s, 1H), 7.65 – 7.54 (m, 2H), 7.53 – 7.29 (m, 2H), 7.12 – 6.98 (m, 4H), 6.92 (dq, J = 7.5, 0.8 Hz, 1H), 6.57 – 6.41 (m, 2H), 6.30 – 5.92 (m, 2H), 5.05 (ddd, J = 12.8, 5.6, 1.3 Hz, 1H), 4.67 (s, 1H), 4.33 (s, 4H), 3.74 – 3.64 (m, 1H), 3.36 (dd, J = 8.7, 5.8 Hz, 2H), 3.31 – 3.24 (m, 2H), 3.14 – 2.97 (m, 4H), 2.88 (ddd, J = 16.8, 13.8, 5.4 Hz, 1H), 2.62 – 2.52 (m, 2H), 2.02 (ddd, J = 13.1, 6.5, 4.2 Hz, 2H), 1.58 (h, J = 7.0 Hz, 2H), 1.45 (dq, J = 11.3, 7.2 Hz, 2H), 1.34 (dq, J = 15.6, 8.0, 7.0 Hz, 2H). LRMS (ESI) calculated for $[M+H]^+$ 779.26, found 778.71.

(3S)-3-((2-chloro-5-(2,2-difluoroethyl)-8-fluoro-5H-dibenzo[b,e][1,4]diazepin-11-yl)amino)-N-(8-((2-(2,6-dioxopiperidin-3-yl)-1,3-dioxoisoindolin-4-yl)amino)octyl)pyrrolidine-1-carboxamide **BJG-05-039**

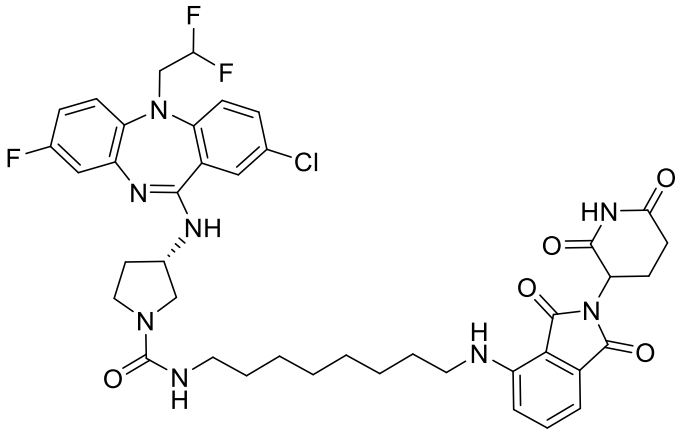

To a solution of solution of 4-((8-aminooctyl)amino)-2-(2,6-dioxopiperidin-3-yl)isoindoline-1,3-dione (20.4 mg, 0.040 mmol, 1 equiv) and (S)-1-(3-((2-chloro-5-(2,2-difluoroethyl)-8-fluoro-5H-dibenzo[b,e][1,4]diazepin-11-yl)amino)pyrrolidine-1-carbonyl)-3-methyl-1H-imidazol-3-ium iodide (25.2 mg, 0.040 mmol, 1 equv) in dichloromethane (0.5 mL), triethylamine (13.9 uL, 0.100 mmol, 2.5 equiv) was added. After 16 hours of stirring, the reaction mixture was rotovapped and diluted with 1.0 mL of N, N-dimethylformamide and purified by reverse-phase prep HPLC (95-15% H_2O/MeOH, 40 mL/min, 45 min). Lyophilization from H_2O/MeCN provided the title compound as a yellow powder (7.8 mg, 24% yield TFA salt).

^{1}H NMR (500 MHz, DMSO-d_6) δ 11.09 (s, 1H), 7.71 (d, J = 9.2 Hz, 1H), 7.64 – 7.49 (m, 3H), 7.48 – 7.35 (m, 1H), 7.16 – 7.08 (m, 2H), 7.02 (d, J = 7.0 Hz, 1H), 6.51 (s, 1H), 6.25 – 5.96 (m, 2H), 5.05 (dd, J = 12.7, 5.4 Hz, 1H), 4.68 (s, 1H), 4.44 – 4.12 (m, 2H), 3.68 (ddd, J = 14.0, 11.1, 6.1 Hz, 1H), 3.39 – 3.31 (m, 2H), 3.28 (t, J = 7.5 Hz, 3H), 3.05 – 2.95 (m, 2H), 2.88 (ddd, J = 16.8, 13.7, 5.4 Hz, 1H), 2.64 – 2.52 (m, 2H), 2.39 – 2.15 (m, 2H), 2.09 – 1.96 (m, 2H), 1.61 – 1.51 (m, 2H), 1.45 – 1.21 (m, 10H). LRMS (ESI) calculated for $[M+H]^+$ 821.21, found 821.15.

(S)-3-((2-chloro-5-(2,2-difluoroethyl)-8-fluoro-5H-dibenzo[b,e][1,4]diazepin-11-yl)amino)-N-(8-(((S)-1-((2S,4R)-4-hydroxy-2-(((S)-1-(4-(4-methylthiazol-5-yl)phenyl)ethyl)carbamoyl)pyrrolidin-1-yl)-3,3-dimethyl-1-oxobutan-2-yl)amino)-8-oxooctyl)pyrrolidine-1-carboxamide **BJG-05-052**

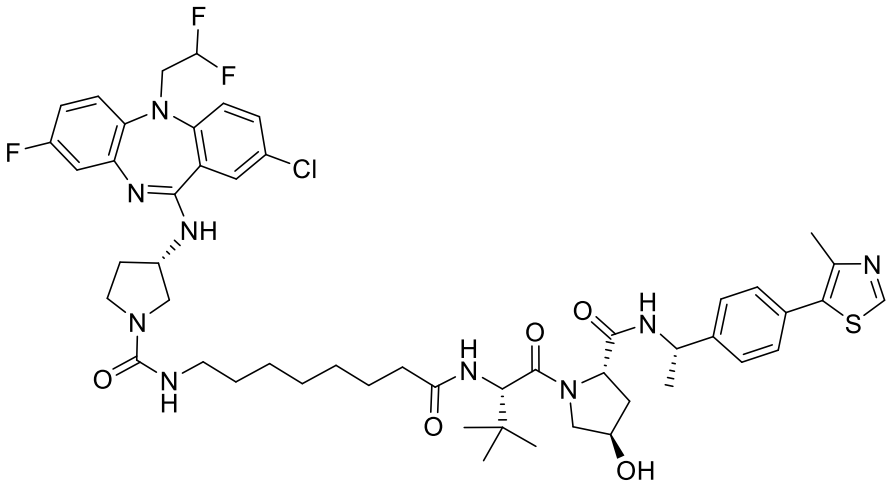

To a solution of solution of (2S,4R)-1-((S)-2-(8-aminooctanamido)-3,3-dimethylbutanoyl)-4-hydroxy-N-((S)-1-(4-(4-methylthiazol-5-yl)phenyl)ethyl)pyrrolidine-2-carboxamide (20.9 mg, 0.030 mmol, 1 equiv) and (S)-1-(3-((2-chloro-5-(2,2-difluoroethyl)-8-fluoro-5H-dibenzo[b,e][1,4]diazepin-11-yl)amino)pyrrolidine-1-carbonyl)-3-methyl-1H-imidazol-3-ium iodide (18.9 mg, 0.030 mmol, 1 equv) in dichloromethane (0.3 mL), triethylamine (10.5 uL, 0.075 mmol, 2.5 equiv) was added. After 16 hours of stirring, the reaction mixture was rotovapped and diluted with 1.0 mL of N, N-dimethylformamide and purified by reverse-phase prep HPLC (95-15% H_2O/MeOH, 40 mL/min, 45 min). Lyophilization from H_2O/MeCN provided the title compound as a white powder (4.3 mg, 14% yield TFA salt).

^{1}H NMR (500 MHz, DMSO-d_6) δ 8.98 (s, 1H), 8.37 (dd, J = 7.9, 1.6 Hz, 1H), 7.77 (dd, J = 9.3, 1.9 Hz, 1H), 7.66 – 7.50 (m, 2H), 7.47 – 7.31 (m, 6H), 6.77 (s, 1H), 6.23 – 5.81 (m, 2H), 5.09 (s, 1H), 4.91 (p, J = 7.1 Hz, 1H), 4.56 (s, 1H), 4.51 (dd, J = 9.4, 2.6 Hz, 1H), 4.42 (td, J = 8.0, 1.8 Hz, 1H), 4.35 – 3.98 (m, 3H), 3.72 – 3.53 (m, 3H), 3.52 – 3.43 (m, 1H), 2.99 (dtd, J = 17.5, 11.4, 10.9, 7.3 Hz, 2H), 2.45 (d, J = 0.9 Hz, 3H), 2.29 – 1.94 (m, 5H), 1.79 (ddd, J = 12.9, 8.5, 4.7 Hz, 1H), 1.56 – 1.32 (m, 8H), 1.23 (t, J = 6.6 Hz, 8H), 0.93 (s, 9H). LRMS (ESI) calculated for $[M+H]^+$ 1006.43, found 1005.73.

(S)-3-((2-chloro-5-(2,2-difluoroethyl)-8-fluoro-5H-dibenzo[b,e][1,4]diazepin-11-yl)amino)-N-(2-(2-(3-(((S)-1-((2S,4R)-4-hydroxy-2-(((S)-1-(4-(4-methylthiazol-5-yl)phenyl)ethyl)carbamoyl)pyrrolidin-1-yl)-3,3-dimethyl-1-oxobutan-2-yl)amino)-3-oxopropoxy)ethoxy)ethyl)pyrrolidine-1-carboxamide **BJG-05-053**

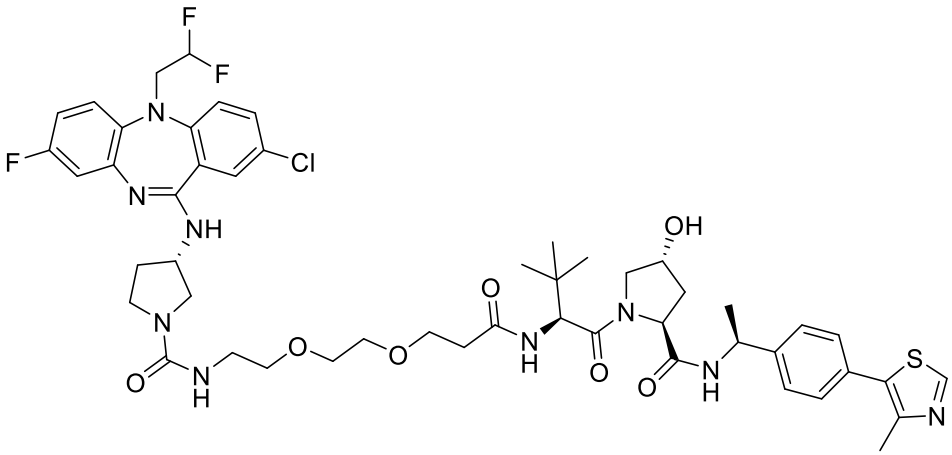

To a solution of solution of (2S,4R)-1-((S)-2-(3-(2-(2-aminoethoxy)ethoxy)propanamido)-3,3-dimethylbutanoyl)-4-hydroxy-N-((S)-1-(4-(4-methylthiazol-5-yl)phenyl)ethyl)pyrrolidine-2-carboxamide (21.5 mg, 0.030 mmol, 1 equiv) and (S)-1-(3-((2-chloro-5-(2,2-difluoroethyl)-8-fluoro-5H-dibenzo[b,e][1,4]diazepin-11-yl)amino)pyrrolidine-1-carbonyl)-3-methyl-1H-imidazol-3-ium iodide (18.9 mg, 0.030 mmol, 1 equv) in dichloromethane (0.3 mL), triethylamine (10.5 uL, 0.075 mmol, 2.5 equiv) was added. After 16 hours of stirring, the reaction mixture was rotovapped and diluted with 1.0 mL of N, N-dimethylformamide and purified by reverse-phase prep HPLC (95-15% H_2O/MeOH, 40 mL/min, 45 min). Lyophilization from H_2O/MeCN provided the title compound as a white powder (4.9 mg, 16% yield TFA salt).

^{1}H NMR (500 MHz, DMSO-d_6) δ 8.98 (d, J = 1.1 Hz, 1H), 8.38 (d, J = 7.7 Hz, 1H), 7.86 (dd, J = 9.3, 1.9 Hz, 1H), 7.66 (s, 1H), 7.60 – 7.26 (m, 7H), 6.33 – 5.87 (m, 2H), 4.91 (p, J = 7.0 Hz, 1H), 4.60 (s, 1H), 4.53 (dd, J = 9.3, 2.1 Hz, 1H), 4.42 (t, J = 8.1 Hz, 1H), 4.37 – 4.10 (m, 3H), 3.64 – 3.57 (m, 6H), 3.43 – 3.26 (m, 7H), 3.22 – 3.12 (m, 2H), 2.45 (d, J = 1.2 Hz, 3H), 2.40 – 2.09 (m, 3H), 2.06 – 1.95 (m, 2H), 1.79 (ddd, J = 12.9, 8.5, 4.7 Hz, 1H), 1.37 (d, J = 7.0 Hz, 3H), 0.93 (s, 9H). (PEG and pyrrolidine methylene protons obscured by water peak). LRMS (ESI) calculated for $[M+H]^+$ 1024.41, found 1023.79.

(3S)-3-((2-chloro-5-(2,2-difluoroethyl)-8-fluoro-5H-dibenzo[b,e][1,4]diazepin-11-yl)amino)-N-(8-((2-(1-methyl-2,6-dioxopiperidin-3-yl)-1,3-dioxoisoindolin-4-yl)amino)octyl)pyrrolidine-1-carboxamide **BJG-05-098** (Negative control of BJG-03-039)

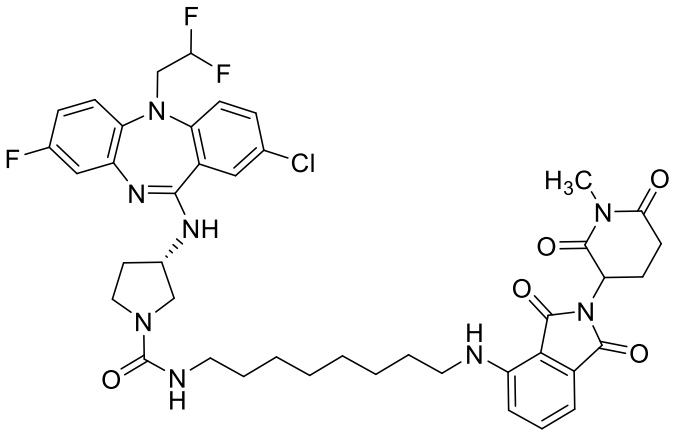

To a solution of solution of 4-((8-aminooctyl)amino)-2-(1-methyl-2,6-dioxopiperidin-3-yl)isoindoline-1,3-dione (17.4 mg, 0.030 mmol, 1 equiv) and (S)-1-(3-((2-chloro-5-(2,2-difluoroethyl)-8-fluoro-5H-dibenzo[b,e][1,4]diazepin-11-yl)amino)pyrrolidine-1-carbonyl)-3-methyl-1H-imidazol-3-ium iodide (18.9 mg, 0.030 mmol, 1 equv) in dichloromethane (0.3 mL), triethylamine (10.5 uL, 0.075 mmol, 2.5 equiv) was added. After 16 hours of stirring, the reaction mixture was rotovapped and diluted with 1.0 mL of N, N-dimethylformamide and purified by reverse-phase prep HPLC (95-15% H_2O/MeOH, 40 mL/min, 45 min). Lyophilization from H_2O/MeCN provided the title compound as a yellow powder (7.1 mg, 28% yield TFA salt).

1H NMR (500 MHz, DMSO-d6) δ 7.61 – 7.45 (m, 3H), 7.39 – 7.28 (m, 2H), 7.13 – 7.05 (m, 2H), 7.02 (d, J = 7.0 Hz, 1H), 6.76 – 6.62 (m, 2H), 6.52 (t, J = 5.9 Hz, 1H), 6.12 – 5.83 (m, 2H), 5.11 (dt, J = 13.1, 5.3 Hz, 1H), 4.51 (td, J = 10.4, 9.6, 4.8 Hz, 1H), 4.26 – 3.95 (m, 2H), 3.60 (ddd, J = 27.3, 10.5, 6.3 Hz, 1H), 3.49 – 3.33 (m, 1H), 3.29 – 3.16 (m, 3H), 3.01 (s, 3H), 3.00 – 2.89 (m, 2H), 2.75 (ddd, J = 17.1, 4.5, 2.6 Hz, 1H), 2.59 – 2.52 (m, 1H), 2.22 – 1.90 (m, 3H), 1.55 (q, J = 7.3 Hz, 2H), 1.45 – 1.14 (m, 12H). LRMS (ESI) calculated for $[M+H]^+$ 835.32, found 834.71.

Synthetic Scheme 3: ATP-competitive degraders

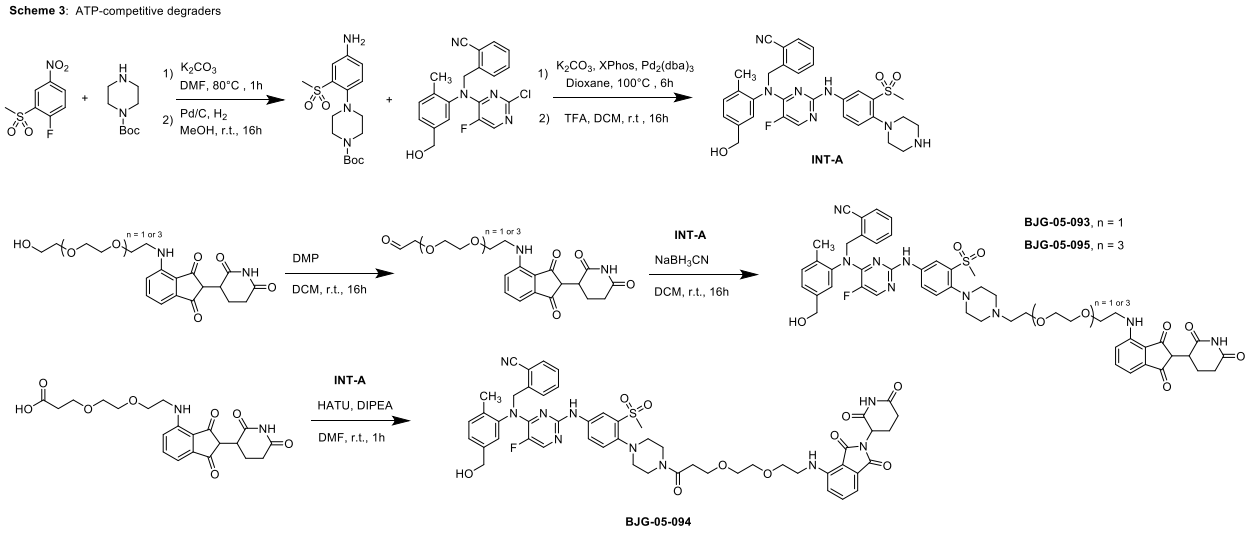

Tert-butyl 4-(4-amino-2-(methylsulfonyl)phenyl)piperazine-1-carboxylate

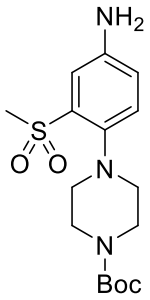

A suspension of 1-fluoro-2-(methylsulfonyl)-4-nitrobenzene (767 mg, 3.5 mmol, 1.0 equiv), tert-butyl piperazine-1-carboxylate (1.956 g, 10.5 mmol, 3.0 equiv), and potassium carbonate (967 mg, 7.0 mmol, 2.0 equiv) in N, N-dimethylformamide (7.0 ml) was stirred at 80°C for 1 hour. The reaction mixture was diluted with ethyl acetate (100 ml), washed with 0.5M HCl, followed by H_2O (3x). The organic fractions were combined, washed with brined, dried over $MgSO_4$, filtered and concentrated in vacuo, yielding 1.355g of yellow solid (~93% purity by NMR). To a suspension of the crude solids in methanol (25 ml), 10 wt % Pd/C (355 mg, 0.35 mmol, 0.1 equiv) was added. The reaction mixture was sparged with H_2 gas for 7 minutes then stirred at room temperature for 16 hours. The mixture was filtered through celite, washing with MeOH (50 ml), and filtrate was concentrated to afford the title compound as a light brown powder (1.248 g, 99% yield, >90 % purity by UPLC-MS). LRMS: $[M+H]^+$ found 355.97

2-(((5-fluoro-2-((3-(methylsulfonyl)-4-(piperazin-1-yl)phenyl)amino)pyrimidin-4-yl)(5-(hydroxymethyl)-2-methylphenyl)amino)methyl)benzonitrile

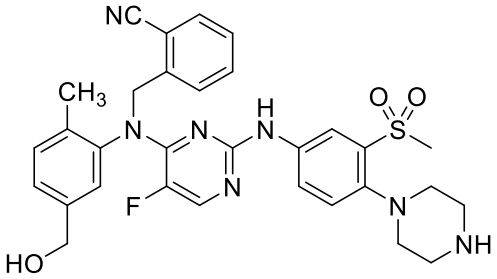

A suspension of 2-(((2-chloro-5-fluoropyrimidin-4-yl)(5-(hydroxymethyl)-2-methylphenyl)amino)methyl)benzonitrile (synthesized according to literature[2]) (765 mg, 2.0 mmol, 1 equiv), tert-butyl 4-(4-amino-2-(methylsulfonyl)phenyl)piperazine-1-carboxylate (781 mg, 2.2 mmol, 1.1 equiv), Tris(dibenzylideneacetone)dipalladium(0) (91.6 mg, 0.10 mmol, 0.05 equiv), XPhos (95.3 mg, 0.20 mmol, 0.10 equiv), and potassium carbonate (829 mg, 6.0 mmol, 3.0 equiv) in dioxane (20 ml) was sparged with N_2 for 10 minutes. The reaction mixture was then stirred at 100°C for 6 hours. After cooling to room temperature, the mixture was filtered through celite, washing with ethyl acetate (50 ml), and concentrated in vacuo. The crude material was purified via silica gel chromatography (30% -> 100% ethyl acetate/hexanes) to afford 1.025g of the boc-protected intermediate (beige solids, LRMS: $[M+H]^+$ found 701.90). To a suspension of boc-protected intermediate in dichloromethane (5 ml), TFA (1 ml) was added. The reaction mixture was stirred at room temperature for 16 hours. The reaction mixture was concentrated in vacuo to afford the title compound (1.563 g, 73% yield over 2 steps). LRMS: $[M+H]^+$ found 601.81)

2-(((2-((4-(4-(2-(2-(2-((2-(2,6-dioxopiperidin-3-yl)-1,3-dioxoisoindolin-4-yl)amino)ethoxy)ethoxy)ethyl)piperazin-1-yl)-3-(methylsulfonyl)phenyl)amino)-5-fluoropyrimidin-4-yl)(5-(hydroxymethyl)-2-methylphenyl)amino)methyl)benzonitrile **BJG-05-093**

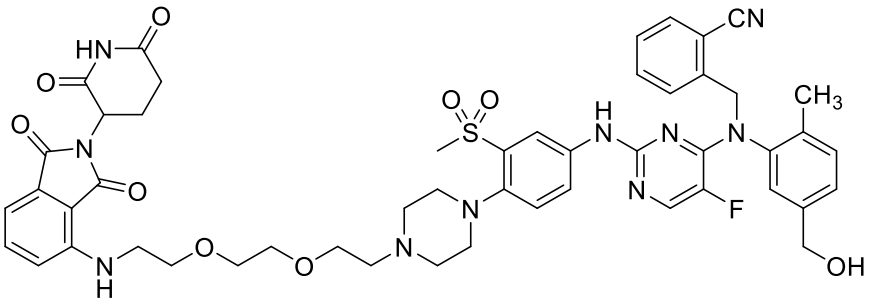

To a solution of solution of 2-(2,6-dioxopiperidin-3-yl)-4-((2-(2-(2-hydroxyethoxy)ethoxy)ethyl)amino)isoindoline-1,3-dione (20.3 mg, 0.050 mmol, 1 equiv) in dichloromethane (1.0 mL), dess-martin periodane (31.8 mg, 0.075 mmol, 1.5 equiv) was added. After 16 hours of stirring at room temperature, the reaction mixture was diluted with 5.0 mL of

dichloromethane, filtered and concentrated. To a solution of the crude aldehyde and 2-(((5-fluoro-2-((3-(methylsulfonyl)-4-(piperazin-1-yl)phenyl)amino)pyrimidin-4-yl)(5-(hydroxymethyl)-2-methylphenyl)amino)methyl)benzonitrile (24.9 mg, 0.030 mmol, 1 equiv) in methanol (0.60 ml), sodium cyanoborohydride (5.6 mg, 0.090 mmol, 3 equiv) was added. After 16 hours of stirring at room temperature, the reaction mixture was diluted with 2.0 mL of methanol, filtered and purified by reverse-phase prep HPLC (95-15% H_2O/MeOH, 40 mL/min, 45 min). Lyophilization from H_2O/MeCN provided the title compound as a yellow powder (8.8 mg, 18% yield TFA salt).

^{1}H NMR (500 MHz, DMSO-d_6) δ 11.09 (s, 1H), 9.65 (s, 1H), 8.29 (s, 1H), 8.02 (d, J = 5.6 Hz, 1H), 7.78 (d, J = 7.7 Hz, 2H), 7.71 – 7.60 (m, 2H), 7.58 (dd, J = 8.6, 7.1 Hz, 1H), 7.45 (td, J = 7.5, 1.5 Hz, 1H), 7.31 (d, J = 8.8 Hz, 1H), 7.23 – 7.12 (m, 3H), 7.06 – 6.99 (m, 2H), 6.61 (t, J = 5.8 Hz, 1H), 5.52 (s, 1H), 5.12 (t, J = 5.6 Hz, 1H), 5.05 (dd, J = 12.8, 5.4 Hz, 1H), 4.37 (d, J = 5.5 Hz, 2H), 3.67 – 3.44 (m, 11H), 3.30 (s, 3H), 2.94 – 2.80 (m, 3H), 2.62 – 2.51 (m, 3H), 2.03 (s, 3H), 2.01 – 1.98 (m, 1H). LRMS (ESI) calculated for $[M+H]^+$ 989.37, found 988.73.

2-(((2-((4-(4-(3-(2-(2-((2-(2,6-dioxopiperidin-3-yl)-1,3-dioxoisoindolin-4-yl)amino)ethoxy)ethoxy)propanoyl)piperazin-1-yl)-3-(methylsulfonyl)phenyl)amino)-5-fluoropyrimidin-4-yl)(5-(hydroxymethyl)-2-methylphenyl)amino)methyl)benzonitrile **BJG-05-094**

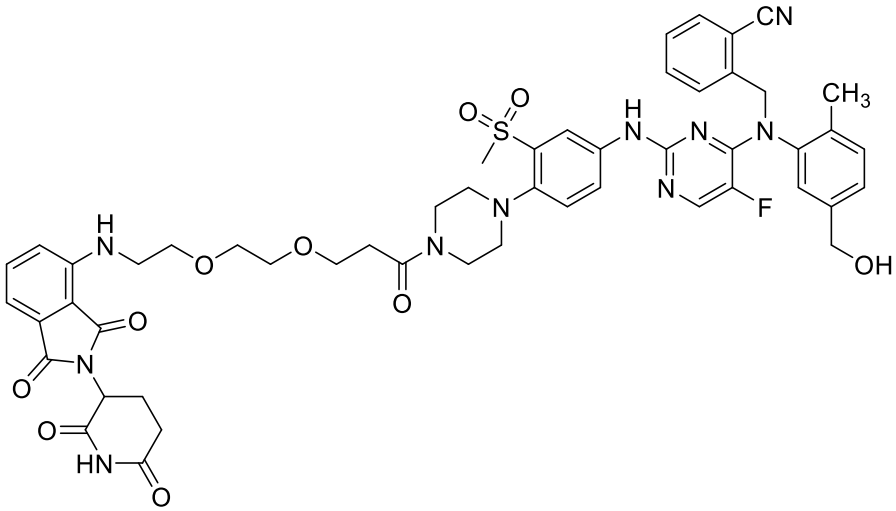

To a solution of solution of 3-(2-(2-((2-(2,6-dioxopiperidin-3-yl)-1,3-dioxoisoindolin-4-yl)amino)ethoxy)ethoxy)propanoic acid (20.7 mg, 0.040 mmol, 1 equiv) in N, N-dimethylformamide (0.5 mL), disopropylamine (34.8 uL, 0.200 mmol, 5 equiv) and HATU (15.2 mg, 0.040 mmol, 1 equiv) were added. After stirring the mixture at room temperature for 5 minutes, 2-(((5-fluoro-2-((3-(methylsulfonyl)-4-(piperazin-1-yl)phenyl)amino)pyrimidin-4-yl)(5-(hydroxymethyl)-2-methylphenyl)amino)methyl)benzonitrile (33.2 mg, 0.040 mmol, 1 equiv) was added. After 2 hours of stirring, the reaction mixture was diluted with 1.0 mL of N, N-dimethylformamide and purified by reverse-phase prep HPLC (95-15% H_2O/MeOH, 40 mL/min, 45 min). Lyophilization from H_2O/ACN provided the title compound as a yellow powder (11.7 mg, 29% yield TFA salt).

^{1}H NMR (500 MHz, DMSO-d_6) δ 11.09 (s, 1H), 9.66 (s, 1H), 8.31 (d, J = 2.6 Hz, 1H), 8.02 (d, J = 5.6 Hz, 1H), 7.78 (dd, J = 7.8, 1.3 Hz, 2H), 7.70 – 7.61 (m, 2H), 7.57 (dd, J = 8.6, 7.0 Hz, 1H), 7.45 (td, J = 7.5, 1.4 Hz, 1H), 7.30 (d, J = 8.7 Hz, 1H), 7.23 – 7.10 (m, 3H), 7.06 – 6.97 (m, 2H), 6.61 (t, J = 5.8 Hz, 1H), 5.52 (s, 1H), 5.11 (t, J = 5.7 Hz, 1H), 5.05 (dd, J = 12.7, 5.4 Hz, 1H), 4.36 (d, J = 5.6 Hz, 2H), 3.69 – 3.60 (m, 4H), 3.60 – 3.50 (m, 5H), 3.46 (q, J = 5.6 Hz, 2H), 2.94 – 2.77 (m, 5H), 2.63 – 2.51 (m, 4H), 2.06 – 1.97 (m, 4H). LRMS (ESI) calculated for $[M+H]^+$ 1017.36, found 1016.63.

2-(((2-((4-(4-(14-((2-(2,6-dioxopiperidin-3-yl)-1,3-dioxoisoindolin-4-yl)amino)-3,6,9,12-tetraoxatetradecyl)piperazin-1-yl)-3-(methylsulfonyl)phenyl)amino)-5-fluoropyrimidin-4-yl)(5-(hydroxymethyl)-2-methylphenyl)amino)methyl)benzonitrile **BJG-05-095**

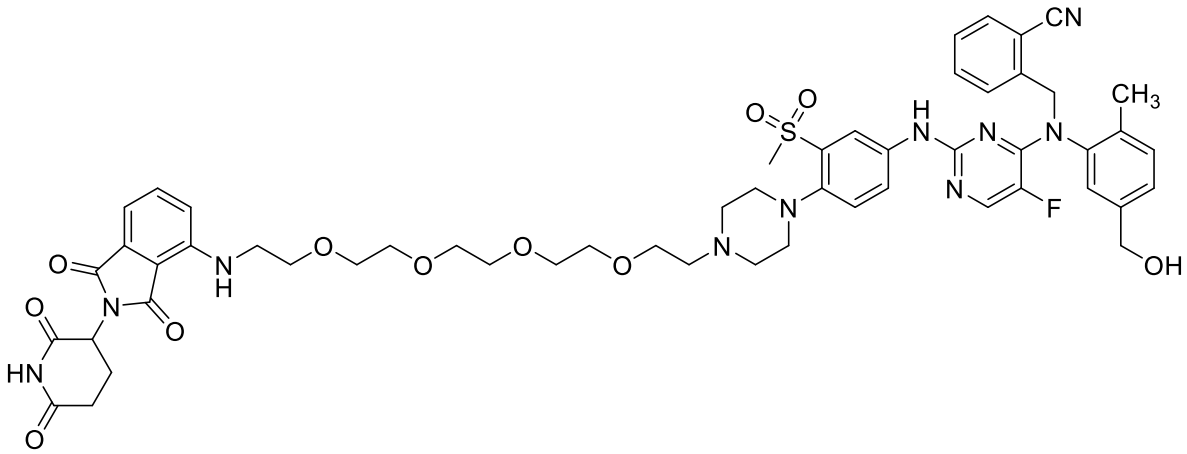

To a solution of solution of 2-(2,6-dioxopiperidin-3-yl)-4-((14-hydroxy-3,6,9,12-tetraoxatetradecyl)amino)isoindoline-1,3-dione (39.5 mg, 0.080 mmol, 1 equiv) in dichloromethane (1.6 mL), dess-martin periodane (50.9 mg, 0.120 mmol, 1.5 equiv) was added. After 16 hours of stirring at room temperature, the reaction mixture was diluted with 5.0 mL of dichloromethane, filtered and concentrated. To a solution of the crude aldehyde and 2-(((5-fluoro-2-((3-(methylsulfonyl)-4-(piperazin-1-yl)phenyl)amino)pyrimidin-4-yl)(5-(hydroxymethyl)-2-methylphenyl)amino)methyl)benzonitrile (66.4 mg, 0.080 mmol, 1 equiv) in methanol (1.0 ml), sodium cyanoborohydride (15.1 mg, 0.240 mmol, 3 equiv) was added. After 16 hours of stirring at room temperature, the reaction mixture was diluted with 2.0 mL of methanol, filtered and purified by reverse-phase prep HPLC (95-15% H_2O/MeOH, 40 mL/min, 45 min). Lyophilization from H_2O/MeCN provided the title compound as a yellow powder (9.6 mg, 11% yield TFA salt).

^{1}H NMR (500 MHz, DMSO-d_6) δ 11.09 (s, 1H), 9.63 (s, 1H), 8.27 (d, J = 2.6 Hz, 1H), 8.01 (d, J = 5.6 Hz, 1H), 7.95 (dd, J = 7.9, 1.2 Hz, 1H), 7.81 – 7.71 (m, 2H), 7.70 – 7.60 (m, 3H), 7.57 (dd, J = 8.6, 7.0 Hz, 1H), 7.45 (td, J = 7.5, 1.3 Hz, 2H), 7.33 (d, J = 8.8 Hz, 1H), 7.23 – 7.15 (m, 3H), 7.13 (d, J = 8.6 Hz, 1H), 7.06 – 6.95 (m, 2H), 6.60 (t, J = 5.8 Hz, 1H), 5.51 (s, 1H), 5.27 – 4.92 (m, 3H), 4.37 (s, 2H), 3.61 (t, J = 5.4 Hz, 2H), 3.59 – 3.42 (m, 20H), 2.95 – 2.81 (m, 5H), 2.62 – 2.55 (m, 1H), 2.07-1.97 (br s, 4H). LRMS (ESI) calculated for $[M+H]^+$ 1077.42, found 1076.65.

References

[1] Karpov, A.S., Amiri, P., Bellamacina, C., Bellance, M.H., Breitenstein, W., Daniel, D., Denay, R., Fabbro, D., Fernandez, C., Galuba, I., et al. (2015). Optimization of a Dibenzodiazepine Hit to a Potent and Selective Allosteric PAK1 Inhibitor. ACS Med. Chem. Lett. 6, 776-781. 10.1021/acsmedchemlett.5b00102

[2] McCoull, W., Hennessy, E. J., Blades, K., Chuaqui, C., Dowling, J. E., Ferguson A. D., Goldberg, F. W., Howe, N., Jones, C. R., Kemmitt, P. D., Lamont, G., Varnes, J. G., Ward, R. A., and Yang, B. (2016). Optimization of Highly Kinase Selective Bis-anilino Pyrimidine PAK1 Inhibitors. ACS Med. Chem. Lett. 7, 1118-1123. https://doi.org/10.1021/acsmedchemlett.6b00322